



Eidgenössische Technische Hochschule Zürich
Swiss Federal Institute of Technology Zurich



Empa

Materials Science and Technology

Semester Thesis

Residual Stress Prediction in SLM Parts: A Sensitivity Analysis

Thordis Tryggvadottir

Supervisor: Prof. Dr. Edoardo Mazza

Co-Supervisor: Dr. Ehsan Hosseini

HTIG, Experimental Continuum Mechanics, Empa
Department of Mechanical and Process Engineering, ETH Zürich

June 21, 2021

Abstract

Additive manufacturing technologies have become more popular in recent years and the need for understanding the processes and their influencing factors has therefore also increased. Finite Element simulations can be used to predict the outcome of a printing process given the input parameters of the process. A fairly recent plug-in developed in ABAQUS by SIMULIA seems to provide good results and easy access for the average user. The underlying mechanisms of the plug-in have not been researched much and it is important to know what is going on in the software so the user knows in which aspects the software can be trusted and where the user must take care. We set up a sensitivity analysis for two models to find how sensitive the software is to a change in the most common parameters of the printing process and find out which methods the software uses to calculate residual stresses in Selective Laser Melting (SLM) printed parts. The first of the two models is a simulation example provided by SIMULIA of a SLM Bridge where a part-level print is observed and the second is a simulation of a single track printed on a substrate where laser movement can be observed. The plug-in calculates the residual stresses using thermal strains and does not require plastic strains to occur to observe residual stress formation in part-level simulations but it can consider plasticity at the process-level. The sensitivity to different process parameters is complex and the results are for most parts inconclusive. A preheating of the base plate results in a lower predicted stress but the effects of laser power and scan speed contrast each other for the different simulation scales.

Acknowledgements

I am very grateful to Prof. Dr. Edoardo Mazza for the opportunity to get to work on this project at the Experimental Continuum Mechanics lab at Empa. I learned a lot throughout the process, I enjoyed working with everyone involved in the project and I could not have managed it without the help of the people involved.

I would like to thank Dr. Ehsan Hosseini for his supervision and assistance throughout the whole process. I really enjoyed working with you.

I want to give special thanks to Mr. Pooriya Gh Ghanbari, who helped me understand the process and topic of the project better and gave me some very good tips and tricks to work with.

In addition, I would like to thank all the employees of the Experimental Continuum Mechanics department at Empa, especially the people in the HTIG, for welcoming me so kindly into their group.

Table of Contents

Abstract.....	ii
Acknowledgements	iii
Table of Contents	iv
List of Figures.....	v
List of Tables.....	vi
List of Abbreviations	vii
1 Introduction	1
2 Theory	2
3 Methods.....	5
3.1 Bridge simulation.....	5
3.1.1 Simulation setup	5
3.2 Single-track simulation	10
3.2.1 Simulation setup	10
4 Results	16
4.1 Bridge.....	16
4.1.1 Reference results.....	16
4.1.2 Sensitivity analysis	18
4.2 Single track	24
4.2.1 Reference results.....	24
4.2.2 Sensitivity analysis	27
5 Conclusions	33
References	35

List of Figures

Figure 3.1: The geometrical setup for the bridge simulation.	5
Figure 3.2: The encastre constraint of the substrate.	7
Figure 3.3: AM setup of bridge simulation.	8
Figure 3.4: The geometrical setup for the simulation of a single track.....	10
Figure 3.5: Constraints for the single-track simulation.	12
Figure 3.6: Meshes of both parts in the single-track simulation.	12
Figure 4.1: Predicted Mises stress of the bridge for the reference configuration.....	16
Figure 4.2: The location of node 9939	17
Figure 4.3: Nodal temperature, Mises stress and pressure for node 9939.....	17
Figure 4.4: The predicted Mises stress profiles of the bridge	18
Figure 4.5: The predicted Mises stress profiles of the bridge	20
Figure 4.6: The predicted Mises stress in the bridge	20
Figure 4.7: The predicted Mises stress profiles of the bridge	21
Figure 4.8: The predicted Mises stress profiles of the bridge	22
Figure 4.9: A graph showing the nodal temperature and Mises stress of node 9939.....	22
Figure 4.10: The location of node 24266	23
Figure 4.11: The nodal temperature of node 24266	23
Figure 4.12: Predicted Mises stress of the single track for the reference configuration	24
Figure 4.13: Approximate melt pool size for the reference configuration	25
Figure 4.14: An example of how the melt pool size changes with varying properties	25
Figure 4.15: The location of node 6792	26
Figure 4.16: Nodal temperature, Mises stress and pressure for node 6792.....	26
Figure 4.17: The predicted Mises stress profiles of the single track	27
Figure 4.18: A path along the centre of printed track.....	28
Figure 4.19: Graph showing the temperature gradient for three different laser power	28
Figure 4.20: The predicted Mises stress profiles of the single track	29
Figure 4.21: Graph showing the temperature gradient for three different scan speeds.....	30
Figure 4.22: The predicted Mises stress profiles of the single track	31
Figure 4.23: Graph showing the temperature gradient for three different initial temp	32

List of Tables

Table 3.1: Material properties used for the bridge simulation	6
Table 3.2: Parameters for reference configuration	9
Table 3.3: Variations of parameters	9
Table 3.4: Material properties used for the single-track simulation.....	11
Table 3.5: Information about simulation settings for different steps and increments	13
Table 3.6: Parameters for reference configuration	14
Table 3.7: Variations of parameters	15
Table 5.1: The effects of increasing the value of different process parameters	33

List of Abbreviations

AM	Additive Manufacturing
FE	Finite Element
FEM	Finite Element Methods
SLM	Selective Laser Melting
TGM	Temperature Gradient Mechanism
TMI	Toolpath-Mesh Intersection Module
EBM	Electron Beam Melting

1 Introduction

Additive Manufacturing (AM) is a concept used for the different manufacturing methods that create parts by adding material units together in contrast to more commonly used subtractive methods that subtract material from an initial block of material. AM technologies – or 3D printing as many people know them – have become very popular in the recent years due to their specific benefits such as rapid prototyping and easy manufacturing of complex geometries and customization.

But even though the technology is very promising, it, as all things, has its flaws and limitations. One of them is the formation of residual stresses that can cause significant distortions in AM parts if they are not accounted for [1]. Since additive manufacturing technologies are rather new not all of the physical processes behind them are known and therefore it is important to try to understand them better to help in determining where the use of AM technologies would be most beneficial.

For that purpose, Finite Element (FE) simulations that predict the outcome of the printing process are valuable tools to try to understand the effects of various parameters on the printing process and the properties of the resulting part. With improved computational power these simulations have become more accessible for people working in the field of additive manufacturing.

ABAQUS by SIMULIA is a software that has recently introduced AM processes as a part of its functions with a plug-in called AM Modeler. The initial aspect of this addition seems to provide convincing results with a reduced computational time compared to some methods since the plug-in framework allows for modelling the different procedures of the printing processes independent of mesh geometry [2]. But even though this user-friendly addition provides an interface making the simulation of AM processes more accessible to the average user it is important to understand the details of the analysis working behind the curtains to evaluate the validity and limitations of the plug-in for different applications.

In this project the goal is to carry out an analysis to try to identify the physical processes that are working behind the curtains in the AM modeler plugin by SIMULIA; which methods the plug-in uses to calculate the given residual stresses of the part and how different process parameters affect the results.

2 Theory

Selective Laser Melting (SLM) is an AM technology developed in the mid-nineties [3] at the Fraunhofer Institute for Laser Technology ILT [4]. It is a printing process that often uses metal powder as the working material that is spread onto a flat surface [4] called a powder bed [5] using a roller or another similar deposition mechanism. To print the part a laser scans a cross-section of the part onto the powder bed, fully melting the powder particles to a substrate that is beneath the powder [4, 5]. This process is repeated until the whole part has been printed [5]. During the printing process high temperature gradients and cooling rates are created which result in the formation of undesired residual stresses in the final printed part [6]. Residual stresses can be defined as stresses that are left in the part after the printing and cooling processes are over [1].

The formation of residual stresses in SLM can be described by two methods. One is the temperature gradient mechanism (TGM). When the material is heated up by the laser it starts to expand but since it is partially inhibited by the material below it cannot expand freely. Compressive stresses start to form which will lead to plastic deformation if yielding occurs. As the laser moves away the material starts to cool down and contract leading to a formation of tensile stresses. The second method considers that the material at the top of the build starts to cool down and contract. Since it is partially inhibited by the material below it will cause tensile stress formation in the top which leads to a compressive stress state in the layers below. [1]

The AM Modeler Plug-in of ABAQUS by SIMULIA provides a convenient user interface where users can easily model AM processes with in-built subroutines and data structures. When modelling AM processes in ABAQUS the Toolpath-mesh intersection module (TMI) can be used for modelling progressive element activation and laser scanning methods through data structures called Event series. [7]

For SLM, material deposition can be defined by an imaginary roller represented by an infinite line in space that is parallel to the printing surface. The location of a central point on the line and the state of the roller are defined for different time points in the event series. The part of an element that is below the intersection plane is considered activated. [7]

To model the laser source either a concentrated point source or a box source with a given distribution such as Goldak or Gaussian can be defined. The former is a valid representation when coarse meshes are used with many printing layers per element, but the latter is more appropriate for fine mesh simulations where there are several elements representing one printing layer. An event series for the power input contains information about the location of the laser source at given times and the source is assumed to have constant properties

between these points. Properties such as laser power can also be defined in the event series. [7]

Other important properties and parameters are defined in data structures called Parameter and Property tables [8]. Parameter tables define the parameters used in the material or power input such as whether a concentrated or box representation is used and the distribution of the laser source [7]. Property tables can include properties such as absorption coefficient [7]. Finally, a table collection is created to connect the relevant structures that are to be used [8].

Although ABAQUS provides some detailed information about how the plug-in takes in the data used for the AM process, there is little information about how it models the output requests such as the residual stresses created in the part and how results compare to experimental results. Two recent studies have shown the promising function of the environment. In 2020 Song et al. [2] used the AM modelling functions of ABAQUS to model two different processes and simulation scales and found that use of the TMI provided good results for the effects of process parameters and surrounding material such as substrate and metal powder, when compared to experimental results. An even more recent publication by An et al. [9] where Electron Beam Melting (EBM) was simulated showed the results using the plug-in were in agreement with results from the literature they were compared to.

For part-level simulations the high temperature gradients and cooling rates cannot be observed properly and therefore a so called relaxation temperature needs to be defined [7]. This temperature is considered as a stress-free temperature and has to be determined by experimental results and calibrated [7]. It is most often somewhere in the range between the annealing and melting temperature of the material [2].

An example of values seen in the literature for preheating temperatures is around 200-400 °C [1, 10] although high temperature preheating of 1500-2500 °C is reported for ceramic materials [11]. Scan speed and laser power values are often in the range of 1000 mm/s and 200-300 W [2, 12].

There are many parameters at play during a printing process and the relationship between them is complex and not fully known [13]. Printing properties such as laser power, scan speed and preheating, material properties such as the relaxation temperature and modelling parameters such as increment size all might affect the resulting outcomes. The effects of the different parameters are not fully known but some results from the literature are reviewed here below.

In 2021 Waqar et al. [6] set up a 3D FEM model for SLM of stainless steel and found that for an increase in either scan speed or laser power the residual stresses increased but kept a similar distribution. These results are supported by experimental results obtained by Mugwagwa et al. [14] for a SLM printed cantilever using Maraging Steel 300.

However, a recent study by Xiao et al. [13] got very inconclusive results with different trends for different laser power and scan speed indicating that the process parameters have complicated effects on the developed residual stress field. They investigated the effects of print parameters on the residual stresses formed by creating a 3D FEM model and comparing it with experiments. Despite the inconclusive results on the effects of each parameter, they managed to rank the parameters by importance of influence on residual stresses as scan speed, laser power and hatch spacing in decreasing order of importance.

For parameters like preheating temperature, Mercelis et al. [1] showed that a preheating of the substrate by 200 °C reduced the residual stresses in the part slightly. The effects of the relaxation temperature on distortion caused by residual stress formation in SLM simulation are reported by Song et al. [2], where a higher relaxation temperature results in greater distortions and residual stresses are therefore considered higher for the increased relaxation temperature.

3 Methods

Two models are set up in ABAQUS, a part-level and a process-level model. Both models are set up as a transient heat transfer analysis with a subsequent static stress analysis that uses the temperature profiles from the heat transfer analysis as input loads, prescribed as predefined fields in ABAQUS. Then an additive manufacturing model is defined with the ABAQUS AM Modeler – Plug-In to simulate the selective laser melting manufacturing of the two models. Finally, a sensitivity analysis is performed for various parameters for both cases.

3.1 Bridge simulation

The bridge model is as part-level simulation based on an example provided by SIMULIA. The simulation focuses on a SLM printed bridge built on a substrate made of the same material. The bridge is made up of twelve narrow columns with two wider ones at both ends and an even wider one in the middle, all connected by overhangs. The geometry and the simulation setup are described in more detail in the following sections.

3.1.1 Simulation setup

Geometry

Figure 3.1 shows the geometry of the bridge used in the simulation. The bridge is approximately $90\text{ mm} \times 20\text{ mm} \times 20\text{ mm}$ printed on the centre of a $280\text{ mm} \times 280\text{ mm} \times 50\text{ mm}$ substrate. The bridge has 15 separate columns that are connected at the top with overhanging structures between them. The outermost columns narrow inwards, so the top of the bridge is smaller than the bottom.

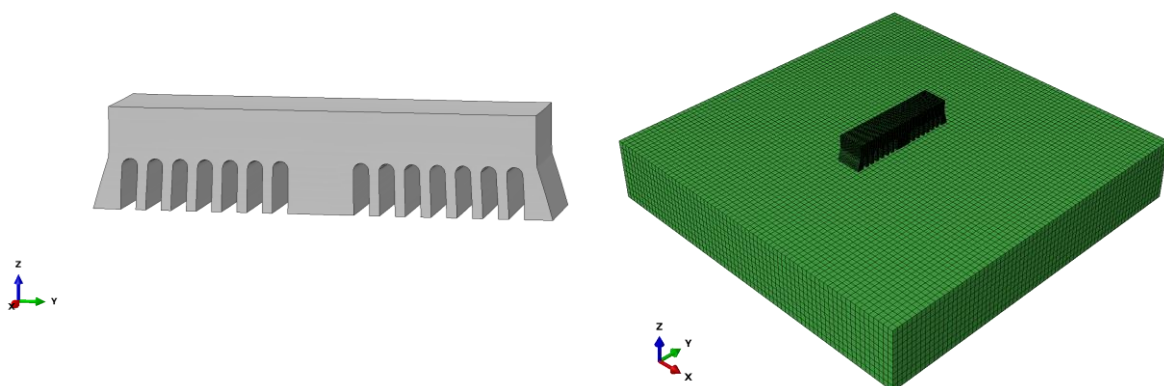


Figure 3.1: The geometrical setup for the bridge simulation. On the left is the SLM bridge where the geometrical features of the bridge can be observed. On the right is the assembly where the bridge can be seen located on top of the bigger substrate.

Material

Both the bridge and the substrate are made of Ti-6Al-4V and modelled with temperature dependent properties for a purely elastic case. The material properties were predefined in the model provided by SIMULIA and have been reproduced in Table 3.1. All material properties are temperature dependant except for the density and all temperatures are given in Kelvins. In addition, the Stefan-Boltzmann constant is defined as $\sigma = 5.67037 \times 10^{-8} \text{ W} \cdot \text{m}^{-2} \cdot \text{K}^{-4}$ and the absolute zero is defined at $T_0 = 0 \text{ K}$. Although all material properties are defined for both analyses, the thermal properties are only used in the heat transfer analysis and the mechanical properties are only used in the stress analysis.

Table 3.1: Material properties used for the bridge simulation. The properties were provided with the model by SIMULIA.

Elastic			Latent Heat			Density	
Young's Modulus [MPa]	Poisson's Ratio	Temp [K]	Latent Heat [J/kg]	Solidus Temp [K]	Liquidus Temp [K]	[kg/m ³]	
104000	0.33	293.15	2.86E+5	1877.15	1923.15	4.43E+03	
101000	0.33	366.15	9.83E+6	3563.15	3663.15		
94000	0.33	478.15					
88300	0.33	588.15					
82600	0.33	698.15					
77500	0.33	813.15					
72600	0.33	923.15					
67400	0.33	1033.15					
62800	0.33	1143.15					
Expansion			Specific Heat		Conductivity		
Expansion Coefficient [m/m·°C]	Temp [K]		Specific Heat [J/kg·K]	Temp [K]	Conductivity [W/m·K]	Temp [K]	
8.60E-06	293.15		5.44E+02	283.15	5.70496	283.15	
8.66E-06	366.15		5.65E+02	383.15	7.27496	383.15	
8.75E-06	478.15		5.87E+02	483.15	8.84496	483.15	
9.08E-06	588.15		6.08E+02	583.15	10.415	583.15	
9.40E-06	698.15		6.30E+02	683.15	11.985	683.15	
9.55E-06	813.15		6.51E+02	783.15	13.555	783.15	
9.70E-06	923.15		6.73E+02	883.15	15.125	883.15	
9.70E-06	1033.15		6.94E+02	983.15	16.695	983.15	
9.70E-06	1143.15		7.16E+02	1083.15	18.265	1083.15	
			7.37E+02	1183.15	19.835	1183.15	
			7.59E+02	1283.15	21.405	1283.15	
			7.80E+02	1383.15	22.975	1383.15	
			8.02E+02	1483.15	24.545	1483.15	
			6.98E+02	1583.15	23.6187	1583.15	
			7.16E+02	1683.15	24.8887	1683.15	
			7.34E+02	1783.15	26.1587	1783.15	
			7.52E+02	1883.15	27.4287	1883.15	

Loads, constraints and initial conditions

To simulate the fusion between the substrate and the bridge a tie constraint is defined to connect them together. The top surface of the substrate is defined as the master surface and the bottom surface of the bridge as the slave surface.

For the mechanical simulation the bottom of the substrate is fixed with an encastre constraint with no movement in any direction as seen in Figure 3.2.

Both the part and the substrate are considered to be at room temperature in the initial configuration. To account for effects of high temperature gradients not observed in this kind of simulation a relaxation temperature of 1200 K is defined.

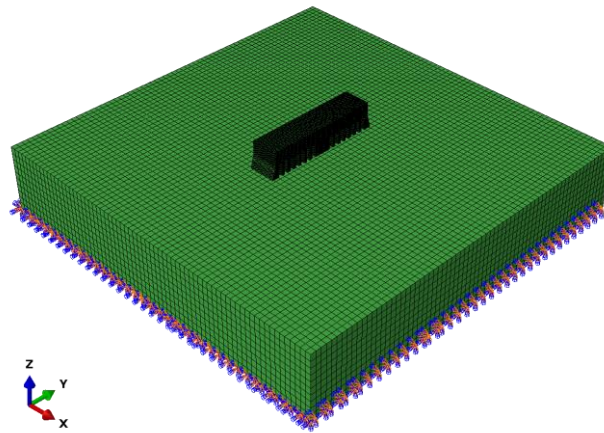


Figure 3.2: The encastre constraint of the substrate.

Mesh and elements

The bridge and the substrate are modelled with linear 8-node brick elements of type DC3D8 for the heat transfer analysis and type C3D8 for the stress analysis. To fill in the mesh of the bridge some linear 6-node triangular prism elements of types DC3D6 and C3D6 are used in the heat transfer and stress analysis respectively. Full integration is used in all cases. For the bridge a mesh size of $1 \text{ mm} \times 0.5 \text{ mm} \times 0.5 \text{ mm}$ is defined and a mesh size of $4 \text{ mm} \times 4 \text{ mm} \times 5 \text{ mm}$ is defined for the substrate.

Steps and increments

In the original model only one step is defined for the whole simulation with an initial increment size of 150 s, allowed to increase to a maximum of 1000 s. To keep the size of the increments even throughout the whole process the maximum size of the increments is decreased to 150 s. All the increments used during the simulation are therefore 150 s except for the last one.

AM setup

To simulate the additive manufacturing process of selectively laser melting the bridge, event series for the material deposition and the laser scanning are defined. The material deposition is modelled as a roller that activates elements that intersect with the layers that are to be printed in each increment. The path of a central point on the roller can be viewed in Figure 3.3. The elements are activated with a full activation and deformations for inactive elements are followed. This means the elements are a part of the model from the start, before they are activated, and can experience deformations but they do not significantly affect the results until after activation [7]. The laser is modelled as a concentrated source with an absorption coefficient of 0.45, scan speed of 1000 mm/s and laser power of 195 W. For cooling effects, a radiation with an emissivity of 0.25 with a sink temperature of 299.15 K is defined along with a convection with a film coefficient of 0.018 also with a sink temperature of 299.15 K. The layer thickness used is 100 μm with five printing layers per element.

The scanning pattern is a raster pattern with the outline scanned last. The pattern rotates by 45° per each printed layer as can be seen in Figure 3.3. The printing process is modelled in a layer-wise manner where several printing layers are activated at once.

The original model provided by SIMULIA does not have any cooling time defined so a cooling time of 80 minutes is added to the printing time. The simulation therefore consists of about 80 minutes of printing and 80 minutes of cooling.

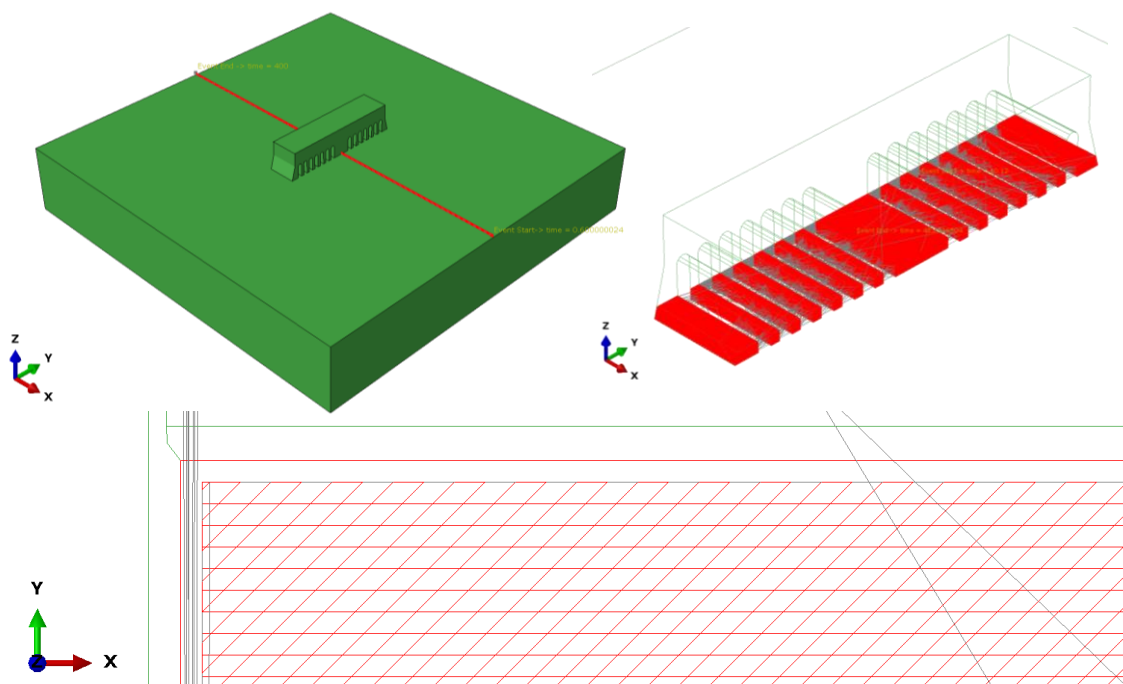


Figure 3.3: AM setup of bridge simulation. In the top left picture, the path of a central point of the roller is visualized. In the top right figure, the scan pattern of several layers is pictured. On the bottom the scan pattern for two layers is showed where the rotation of 45° per layer is visible.

Sensitivity Analysis

The sensitivity analysis is done by running the simulation varying one parameter in each run. The reference parameters for the sensitivity analysis are the parameters that have been described in the previous section and can be viewed again in Table 3.2.

Table 3.2: Parameters for reference configuration used in the sensitivity analysis of the bridge simulation.

Parameter	Value
Laser power	195 W
Scan speed	1000 mm/s
Relaxation temperature	1200 K
Initial temperature	299.15 K
Increment size	150 s
Number of increments	~ 60
Layer thickness	100 μm
Printing time	~ 80 minutes
Cooling time	80 minutes

In the sensitivity analysis the laser power, relaxation temperature, initial temperature and increment size are varied with the properties seen in Table 3.3. The values of the variables were decided partially by looking at common values indicated in the literature and partially by choosing a up and down variation from the reference configuration.

Table 3.3: Variations of parameters in the sensitivity analysis of the bridge simulation.

Parameter	Value 1	Value 2	Value 3
Laser power	100 W	200 W	300 W
Relaxation temperature	299.15 K	1000 K	1200 K
Initial temperature	299.15 K	370 K	870 K
Increment size	150 s	100 s	50 s

It should be noted that for the variation of increment size the cooling time of the part is decreased to 40 minutes to save some computational time. The effects of the length of the cooling time are also investigated by defining a cooling time of 120 minutes and then check when the system is in equilibrium.

3.2 Single-track simulation

The single-track simulation is a process-level simulation focusing on a single track printed on a small and thin substrate. The process-level simulation looks at the printing process in much more detail and can observe the laser movement and high temperature gradients.

3.2.1 Simulation setup

Geometry

The geometry that is used is a replica of a single track sitting on top of a substrate with dimensions $2\text{ mm} \times 150\text{ }\mu\text{m} \times 30\text{ }\mu\text{m}$ and $4\text{ mm} \times 4\text{ mm} \times 0.5\text{ mm}$ respectively and can be seen in Figure 3.4. The track is located at the centre of the substrate.

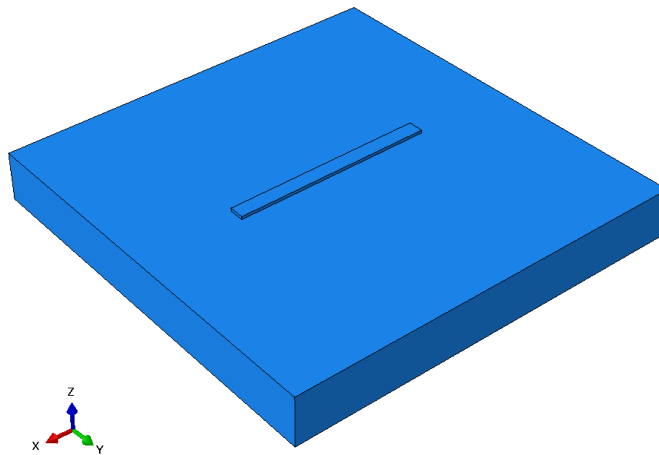


Figure 3.4: The geometrical setup for the simulation of a single track printed on a small substrate.

Material

The material that is used in the simulation is Hastelloy[®] X by Haynes International. Most material properties were adapted from their brochure with room temperature taken at 20 °C [15]. The high temperature values for the conductivity were received in a meeting with Pooriya Gh Ghanbari. He adapted them both from Valencia and Queded [16] and followed Luo and Zhao [17] in their method of increasing the conductivity $\times 15$ to account for the liquid conductivity increase due to melt pool convection (e.g. Marangoni effect). A low yield strength and yield stress are defined for the liquid at high temperatures. The same metal is used for both parts.

For this case perfect plasticity is assumed for the stress analysis and no latent heat is considered. The material properties can be viewed in Table 3.4. In addition, the Stefan-Boltzmann constant is as before with the value obtained from the SIMULIA example as $\sigma = 5.67037 \times 10^{-8} \text{ W} \cdot \text{m}^{-2} \cdot \text{K}^{-4}$ and the absolute zero is defined at $T_0 = -273.15\text{ }^\circ\text{C}$.

Table 3.4: Material properties used for the single-track simulation. Most of the data is from Haynes International [15]. *Value adapted from Valencia and Queded [16] by Pooriya Gh Ghanbari. **Obtained with method from Luo and Zhao [17] by Pooriya Gh Ghanbari. ***Low values added for liquid phase of material.

Density		Elastic			Plastic		
8.22E+03	kg/m ³	Young's Modulus [MPa]	Poisson's Ratio	Temp [K]	Yield Stress [MPa]	Plastic Strain	Temp [K]
		205000	0.32	20	379	0	22
		203000	0.32	93	767	0.44	22
		197000	0.32	204	245	0	538
		192000	0.32	316	614	0.49	538
		184000	0.32	427	244	0	649
		178000	0.32	538	581	0.54	649
		170000	0.32	649	237	0	760
		161000	0.32	760	463	0.53	760
		153000	0.32	871	194	0	871
		141000	0.32	982	310	0.59	871
		10000***	0.32***	2000	91	0	982
					177	0.66	982
					43	0	1093
					97	0.6	1093
					10***	0***	2000
					10***	0.6***	2000
Conductivity		Specific Heat					
Conductivity [W/m·K]	Temp [K]	Specific Heat [J/kg·K]	Temp [K]				
9.2	25	4.86E+02	20				
34.6*	1260	8.58E+02	1093				
500**	2000						
Expansion, zero=26							
Expansion Coefficient [m/m·°C]	Temp [K]						
1.39E-05	93						
1.51E-05	538						
1.55E-05	649						
1.58E-05	732						
1.60E-05	816						
1.64E-05	899						
1.66E-05	982						

Loads and constraints

The substrate and the printed track are modelled as two separate parts connected with a tie constraint. The tie constraint treats the top surface of the substrate as the master surface, as can be seen in Figure 3.5, and the bottom surface of the track as the slave surface. This simulates the fusion of the two parts that occurs during printing.

For the heat transfer analysis, the bottom surface of the substrate is kept at a fixed temperature throughout the analysis and both the substrate and the track are assumed to have

an initial temperature at room temperature. In the stress analysis the bottom surface of the substrate is modelled with all degrees of freedom fixed for zero displacement (see Figure 3.5). In the stress analysis the temperature profile from the heat transfer analysis is defined as a predefined field for loading the part.

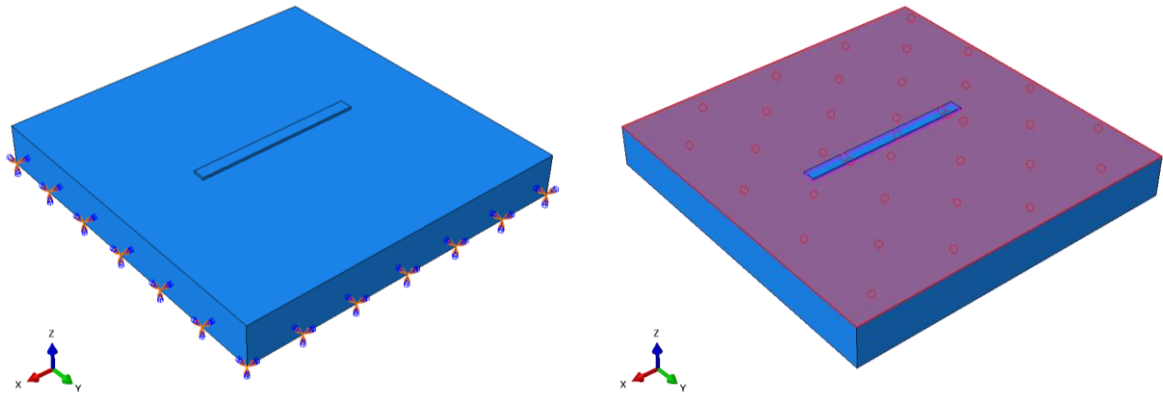


Figure 3.5: Constraints for the single-track simulation. On the left the zero displacement of the bottom surface of the substrate is shown and on the right the master surface for the tie constraint connecting the track and the substrate is shown.

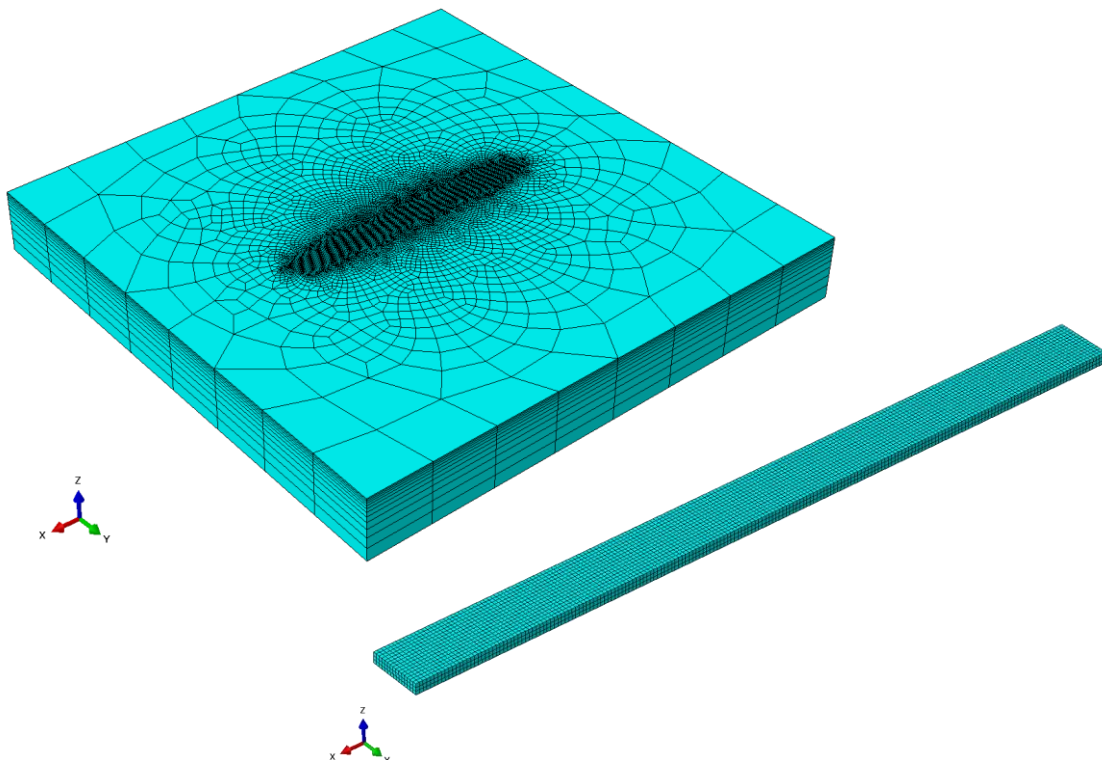


Figure 3.6: Meshes of both parts in the single-track simulation. The substrate matches the fine mesh of the track where the parts meet but the element size is increased with a sweep mesh towards the edges of the substrate to improve computational time. Note that the parts are not shown in the same scale.

Mesh and elements

As mentioned in the previous paragraph the parts are modelled as two separate parts and they are also meshed separately. The track is meshed with evenly sized $10\ \mu\text{m} \times 10\ \mu\text{m} \times 10\ \mu\text{m}$ elements. The mesh for the substrate is created by a sweep mesh that is made to match the track mesh in the region where the two parts connect and through the thickness of the substrate, but the element size is allowed to increase to $500\ \mu\text{m}$ away from the centre and $100\ \mu\text{m}$ in thickness from top to bottom. Figure 3.6 shows how the mesh looks for both parts separately. The same mesh is used for both analyses.

For the heat transfer analysis both the substrate and the track are modelled with 8-node linear heat transfer brick elements of type DC3D8 with full integration. For the mechanical analysis the analogous 8-node linear brick elements of type C3D8 are used with full integration for both parts.

Steps and increments

For both the heat transfer analysis and the stress analysis the simulation is divided into three steps: a deposition step, a laser scanning step and a cooling step. The duration of the steps as well as the increment size control settings can be seen in Table 3.5 for each of the two analyses. The duration of the laser scanning steps defined in the table are based on a scan speed of $1000\ \text{mm/s}$.

Table 3.5: Information about simulation settings for different steps and increments in the two analyses; heat transfer analysis and stress analysis. The duration of the laser scanning step is based on a scan speed of $v=1000\ \text{mm/s}$.

Parameter					
	Duration	Increment Size			Maximum temperature change
		Initial	Minimum	Maximum	
Deposition	3 s	3	3	3	1000 °C
Laser scanning	0.002 s	1e-06	1e-08	0.002	200 °C
Cooling	10 s	1e-06	1e-08	0.2	50 °C
Stress analysis					
	Duration	Increment Size			Maximum temperature change
		Initial	Minimum	Maximum	
Deposition	3 s	3	3	3	-
Laser scanning	0.002 s	1e-05	1e-08	1e-05	-
Cooling	10 s	0.0001	1e-08	0.2	-

In the heat transfer analysis, the deposition step is modelled in one increment since it is the first deposition of the print and no heat has been added to the system at that time and therefore no temperature changes are expected. The laser scanning step has fine increments and a lower allowed temperature change to make sure that the high temperature gradients of the system are modelled correctly. And finally, the cooling step is modelled with bigger increments than the laser scanning but since the duration of this step is quite long the maximum increment size is allowed to go up but to make sure that everything is still under control the maximum allowed temperature change per increment is kept at 50 °C. For the stress analysis similar controls are observed except the initial steps are made a bit bigger to try to improve the computational time of the simulation since the stress analysis takes more computational time than the heat transfer analysis.

AM setup

For modelling the additive manufacturing of the single track, the event series for material deposition and laser scanning are defined. The material deposition is defined in the same way as for the bridge, but the layer thickness is defined as 30 μm . A scan speed of 1000 mm/s and a laser power of 200 W are defined for the reference configuration. The laser source is modelled with a Goldak distribution and the laser is assumed to have an absorptivity of 0.5. For cooling effects, a radiation with emissivity 0.25 with a sink temperature of 26 °C is defined and a convection with a film coefficient of 0.018 also with a sink temperature of 26 °C. Deformations of inactive elements are followed in this case as in the bridge simulation.

Sensitivity analysis

The reference configuration parameters have been described in the previous sections and can be viewed in Table 3.6. The values chosen for the reference configuration are mostly based on the values from the bridge simulation and supported by common values in the literature.

Table 3.6: Parameters for reference configuration used in the sensitivity analysis of the single-track simulation.

Parameter	Value
Laser power	200 W
Scan speed	1000 mm/s
Initial temperature	25 °C
Substrate temperature	25 °C
Layer thickness	30 μm
Deposition time	3 s
Printing time	0.002 s
Cooling time	10 s

In the sensitivity analysis the laser power, scan speed and initial temperature are varied as seen in Table 3.7. The values of the variables were decided partially by looking at common values indicated in the literature and partially by choosing a up and down variation from the reference configuration.

Table 3.7: Variations of parameters for the sensitivity analysis of the single-track simulation.

Parameter	Value 1	Value 2	Value 3
Laser power	100 W	200 W	300 W
Scan speed	800 mm/s	1000 mm/s	1200 mm/s
Initial temperature	25 °C	200 °C	400 °C

4 Results

The simulation models for the sensitivity analysis were run using ABAQUS/2020 by SIMULIA on Euler, the central High-Performance Computing (HPC) cluster of ETH, and the results for the residual Mises stresses formed in the parts are compared for the different models.

4.1 Bridge

4.1.1 Reference results

The results for the reference configuration can be seen in Figure 4.1. The distribution shows quite high residual stresses in the part with the maximum at 7679 MPa for averaged values and few places with very low stresses. The top surface of the bridge has lower residual stresses since the top part is not constrained by the material around it and can move more easily than the layers below making residual stress formation lower. The bottom corners are constrained by the substrate and the material above and experience the highest stress concentration.

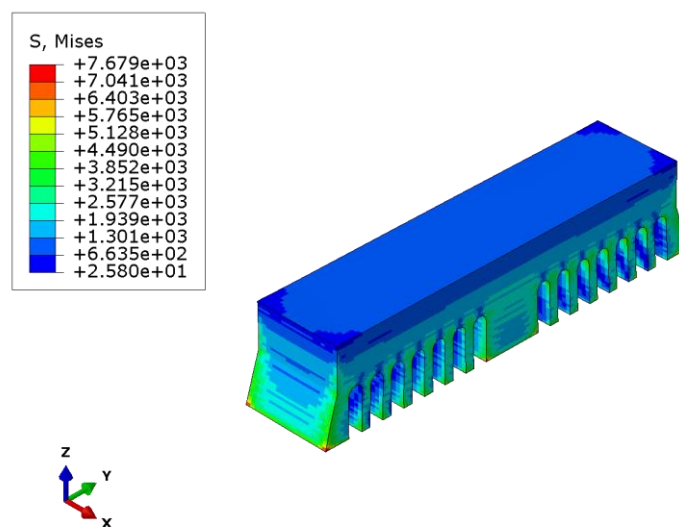


Figure 4.1: Predicted Mises stress of the bridge for the reference configuration for averaged values. The maximum predicted stress can be observed in the bottom corners of the part.

To have a closer look at the stresses formed in the part the nodal temperature, Mises stress and pressure for a node close to the top of the part are plotted over the simulation time. The node in question is node number 9939 and it can be viewed in Figure 4.2.

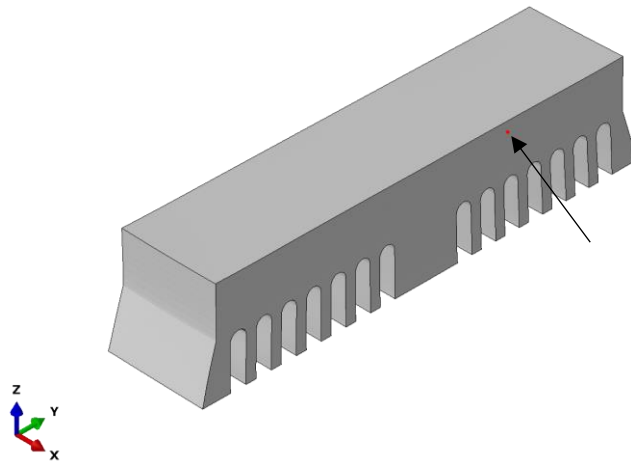


Figure 4.2: The location of node 9939 on the bridge marked with a small red dot, pointed out by the arrow.

The plotted results are visible in Figure 4.3. Since high temperature gradients are not observed the material is defined at the relaxation temperature of 1200 K as an initial condition. The nodal temperature curve displays the initial relaxation temperature that drops down in the graph while the node is inactive. This is not representative of how the temperature value changes, when the node is activated (around the 4000 s mark in the figure) it will still have the high initial temperature value and then drop down to the working temperature of the part creating the residual stresses.

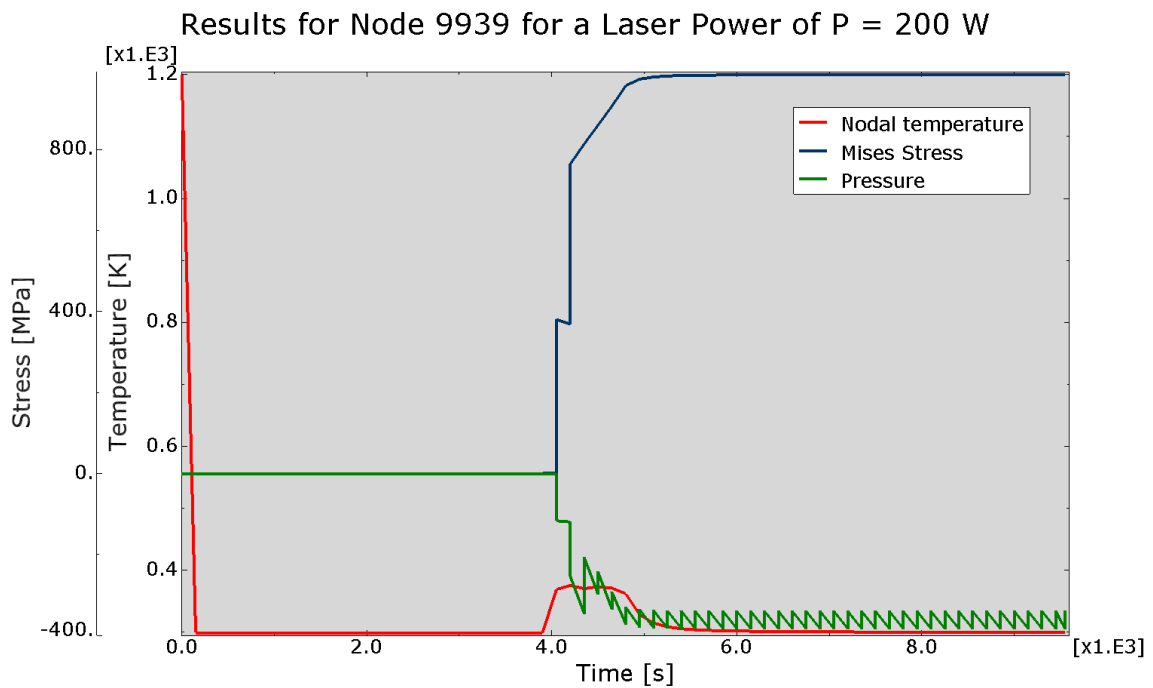


Figure 4.3: Nodal temperature, Mises stress and pressure for node 9939 during the printing process. The fluctuations in the pressure curve occur due to the difference between the calculated pressure values at the integration points for the two element layers connected to the node.

When the node is activated and the temperature drops down, high Mises stresses are formed. By looking at the pressure curve it shows that the pressure is negative for the stresses that form, indicating tensile stress formation as the part cools down and the material contracts. Since the bridge example only considers elastic material behaviour the residual stresses formed are significantly higher than the typical yield strength of Ti-6Al-4V which is for example measured less than 1100 MPa for an SLM printed rod by Shunmugavel et al. [18].

4.1.2 Sensitivity analysis

Power

In Figure 4.4 the predicted Mises stress formed in the bridge for three different laser power can be seen. Both the maximum stress reported in the bridge along with the overall stress distribution clearly decrease with increased laser power.

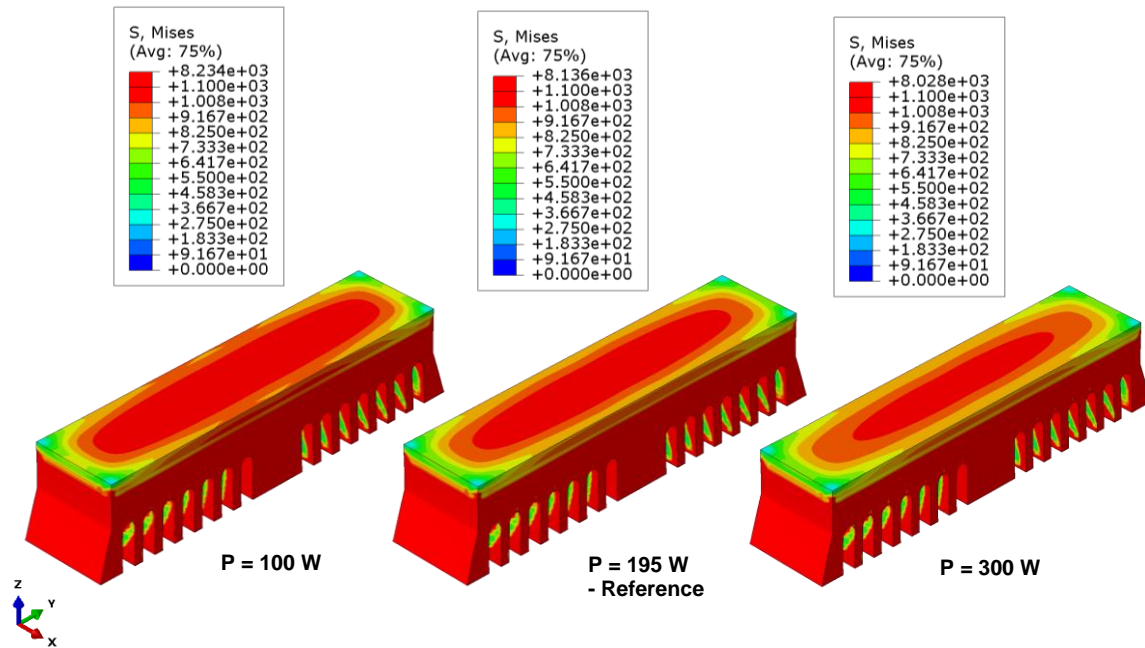


Figure 4.4: The predicted Mises stress profiles of the bridge for three different laser power. A laser power of 100 W on the left, 195 W in the centre and 300 W to the right. The stress decreases with increasing laser power.

As the laser power is increased more energy enters the system resulting in higher temperatures. A higher working temperature of the part means that the gap between the relaxation temperature and the temperature of the part is smaller and as a consequence smaller residual stresses form in the part since it has less cooling down to go through.

Scan speed

No sensitivity analysis was made for the scan speed of the laser. The bridge is printed in a layer-wise manner which means that for each time increment several printing layers are

activated at once and the laser scanning analysed for them all before the next layers are activated. We assume this to mean that when the scan speed is increased it results in a shorter time that the concentrated laser source spends in the system.

For a laser power of 200 W and a scan speed of 1000 mm/s the printing of one layer takes about 10 s and the energy that enters the system is:

$$E_1 = 200 \text{ W} * 10 \text{ s} = 2000 \text{ J}$$

The scanning distance would therefore be:

$$d = 1000 \frac{\text{mm}}{\text{s}} * 10 \text{ s} = 10.000 \text{ mm}$$

If we now double the scan speed to 2000 mm/s the time to scan one layer will be:

$$t = \frac{10.000 \text{ mm}}{2000 \frac{\text{mm}}{\text{s}}} = 5 \text{ s}$$

so half of the original scanning time. It will therefore lead to the energy entering the system to be decreased by half:

$$E_2 = 200 \text{ W} * 5 \text{ s} = 1000 \text{ J}$$

which would amount to the same effects of decreasing the laser power by half.

The effects of the scan speed on the residual stress formation are therefore concluded to be such that an increase in scan speed will lead to a decrease in the residual stresses.

Note that in the calculations above the effects of cooling at the evolving boundaries are neglected. The cooling will have some effect on the results, but the effects are assumed minimal, and the relationship above can be considered mostly valid.

Relaxation temperature

When the relaxation temperature value is varied the resulting predicted Mises stress increases with an increased relaxation temperature value as can be seen in Figure 4.5.

Similarly to what we have for the power, when the relaxation temperature value is increased, the gap between the relaxation temperature and the temperature of the printed part is increased and the elements have too cool down over a bigger gap leading to higher residual stress formations. The difference is clearly visible in Figure 4.5, which points to a high sensitivity to the relaxation temperature value.

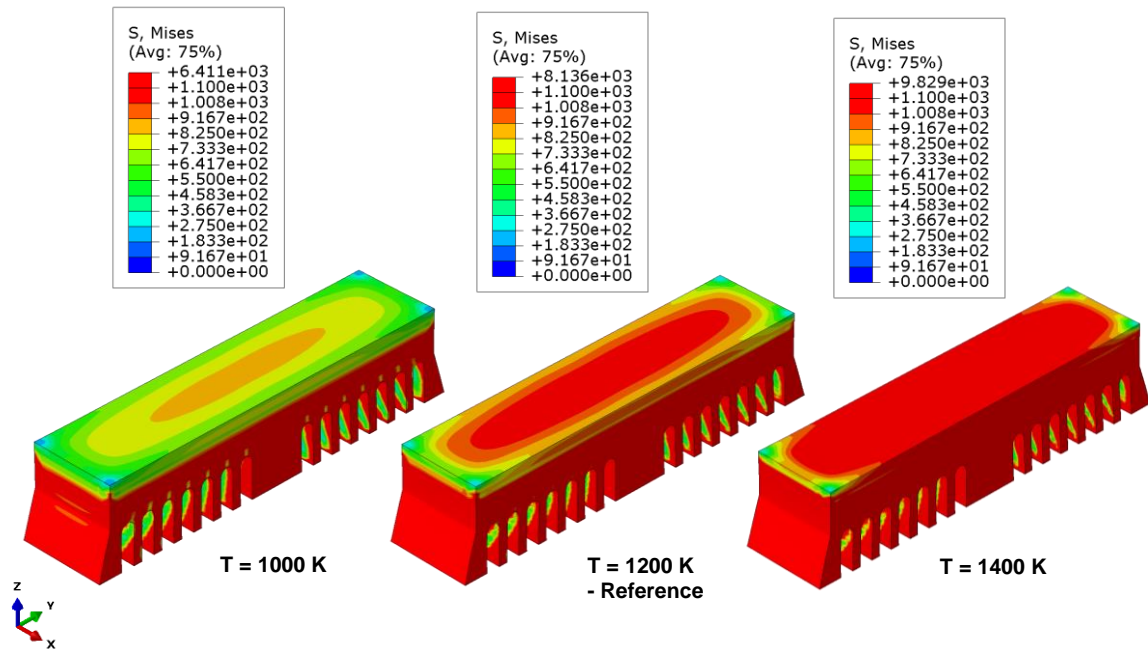


Figure 4.5: The predicted Mises stress profiles of the bridge for three different relaxation temperature values. A relaxation temperature of 1000 K on the left, the reference of 1200 K in the centre and 1400 K to the right. The stress increases with increased relaxation temperature.

Now if the relaxation temperature is ignored, that is the value is set to $T = 299.15$ K almost no residual stresses form in the part as Figure 4.6 shows. The stresses formed in this case are compressive because the relaxation temperature is lower than the working temperature and the elements have to expand to reach the temperature of the part. This shows the importance of including a relaxation temperature in part-level simulations where the high temperature gradients and laser movement cannot be observed.

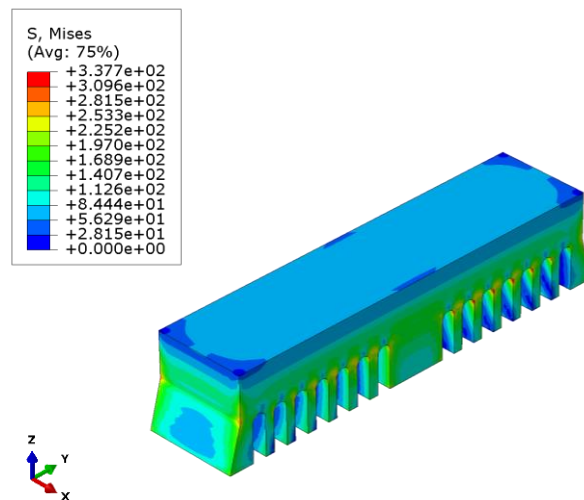


Figure 4.6: The predicted Mises stress in the bridge when the relaxation temperature is ignored. The residual stresses are very low compared to the stresses when the relaxation temperature is included and they also have a different nature being compressive instead of tensile.

Preheating

When the preheating temperature of the bridge is increased the simulation results report a decrease in the residual stresses formed as shown in Figure 4.7.

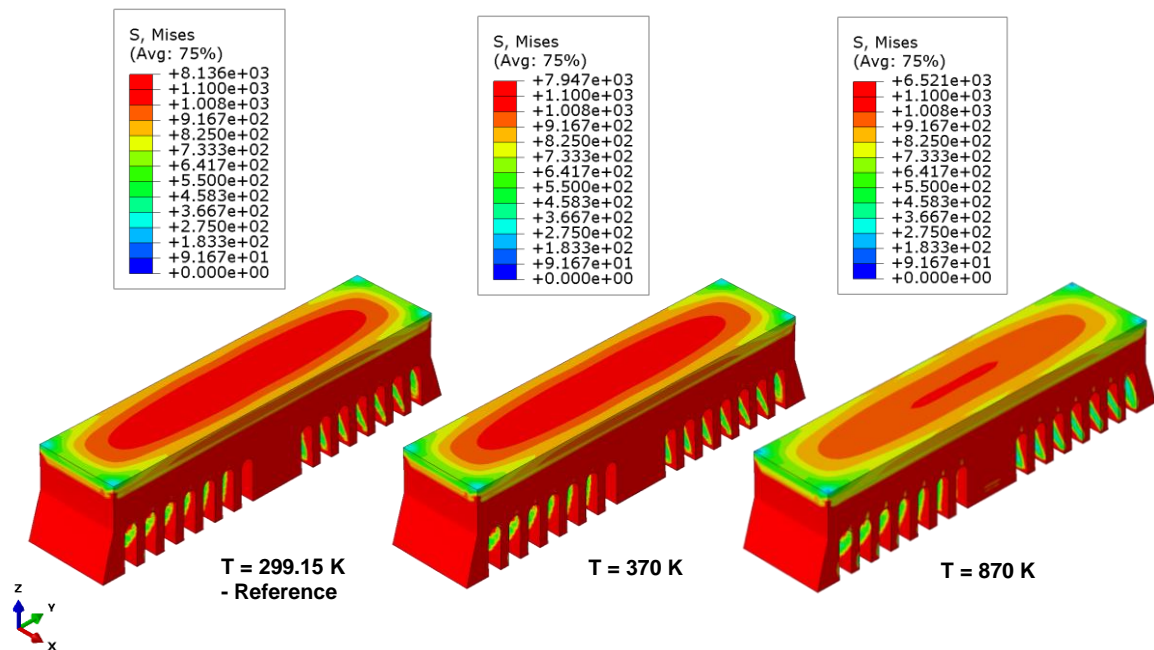


Figure 4.7: The predicted Mises stress profiles of the bridge for three different initial temperature values. The reference of no preheating with an initial temperature at room temperature is shown on the left, a small preheating of $T = 370 \text{ K}$ is shown in the centre and a higher preheating of $T = 870 \text{ K}$ is shown on the right. The stress decreases with increased initial temperature.

These results can be explained in the same way as for the previous two parameters investigated. When the energy enters the system, it will heat the bridge up to a higher temperature. Since the three cases start at a different initial temperature the final temperature will also be different and the gap between the relaxation temperature and the temperature of the bridge will be biggest for the reference configuration and smallest for the case with a preheating of $T = 870 \text{ K}$. Since the gap decreases with increasing preheating temperature, the residual stresses also decrease with an increasing preheating temperature.

Increments

The predicted Mises stress for different increment sizes can be viewed in Figure 4.8. The residual stresses increase with decreasing increment size, that is higher residual stresses form for smaller time increments. To try to explain the results the nodal temperature and Mises stresses for node 9939 (see Figure 4.2) are plotted for increment sizes of $i = 50 \text{ s}$ and $i = 150 \text{ s}$. The data points are very distributed and do not provide a clear reason for the trend. To evaluate the reason for the reported results more time and detailed evaluations are needed.

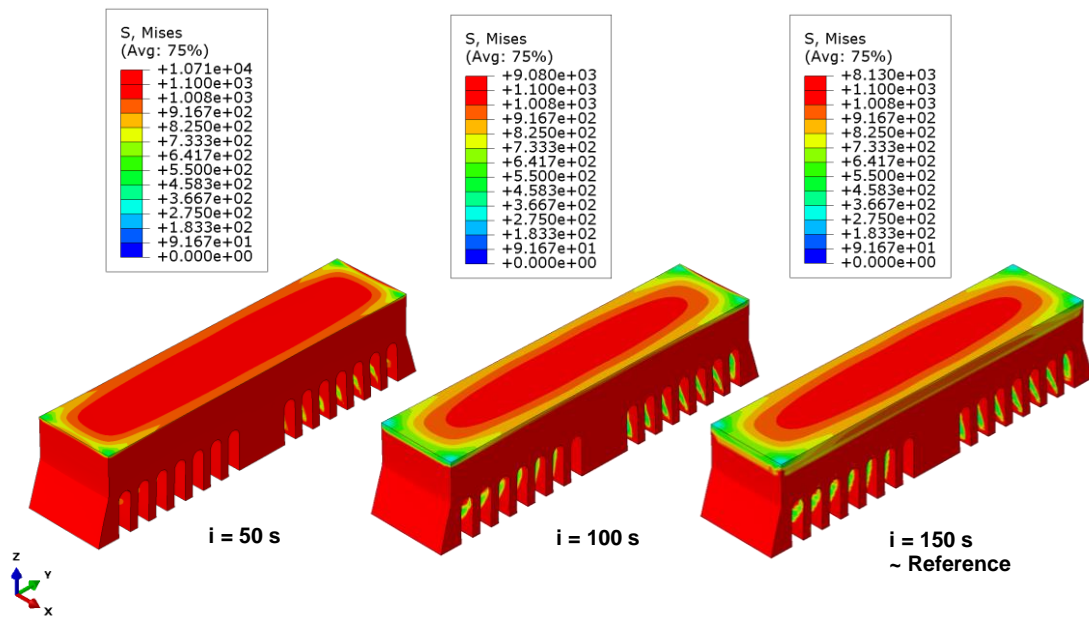


Figure 4.8: The predicted Mises stress profiles of the bridge for three different increment sizes. The smallest increments at $i = 50$ s on the left, increment size of $i = 100$ s in the centre and the reference size of $i = 150$ s on the right. Note that for the increment sensitivity analysis the cooling time was shortened to 40 minutes to improve computational time.

Nodal Temperature and Mises Stress of Node 9939 for Two Increment Sizes

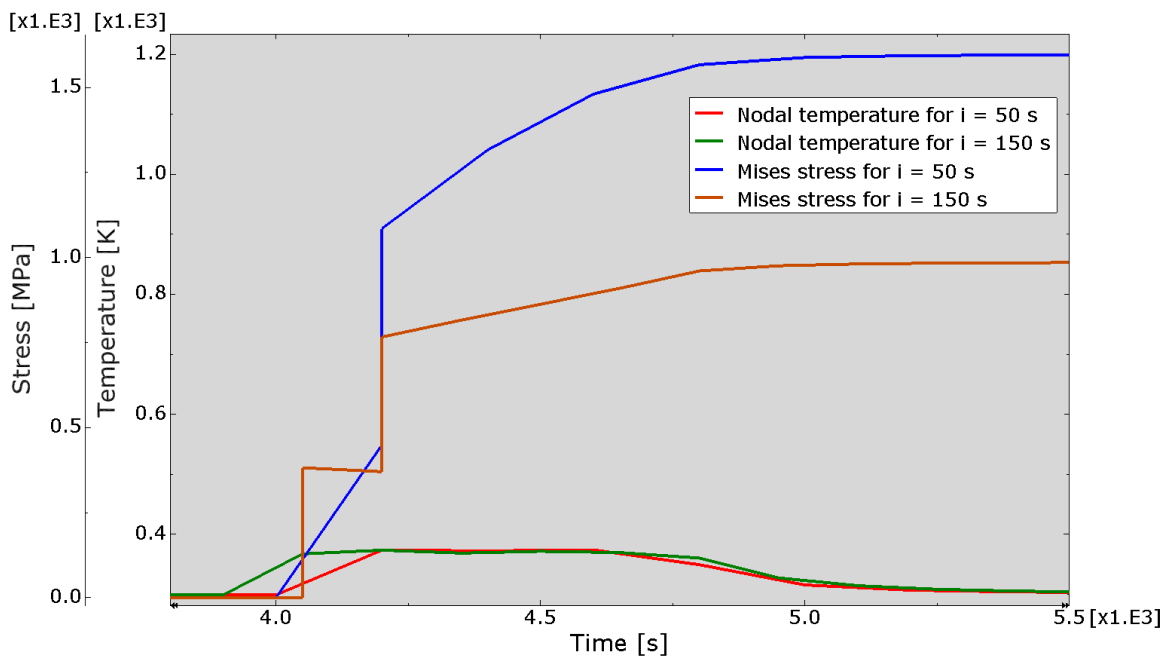


Figure 4.9: A graph showing the nodal temperature and Mises stress of node 9939 pictured in Figure 4.2 for two different increment sizes of $i = 150$ s and $i = 50$ s during a part of the printing time.

Cooling time

The original model provided by SIMULIA did not have any cooling time defined for the process. A cooling time of 80 minutes was added to the reference simulation but to investigate when the system reached an equilibrium a cooling time of 120 minutes was also defined to be investigated. The nodal temperature for node 24266 located in the middle of the bottom of the central column of the bridge (see Figure 4.10) is plotted over the process time.

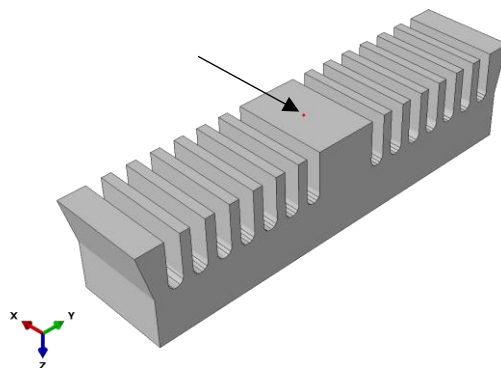


Figure 4.10: The location of node 24266 on the bridge marked with a small red dot, pointed out by the arrow.

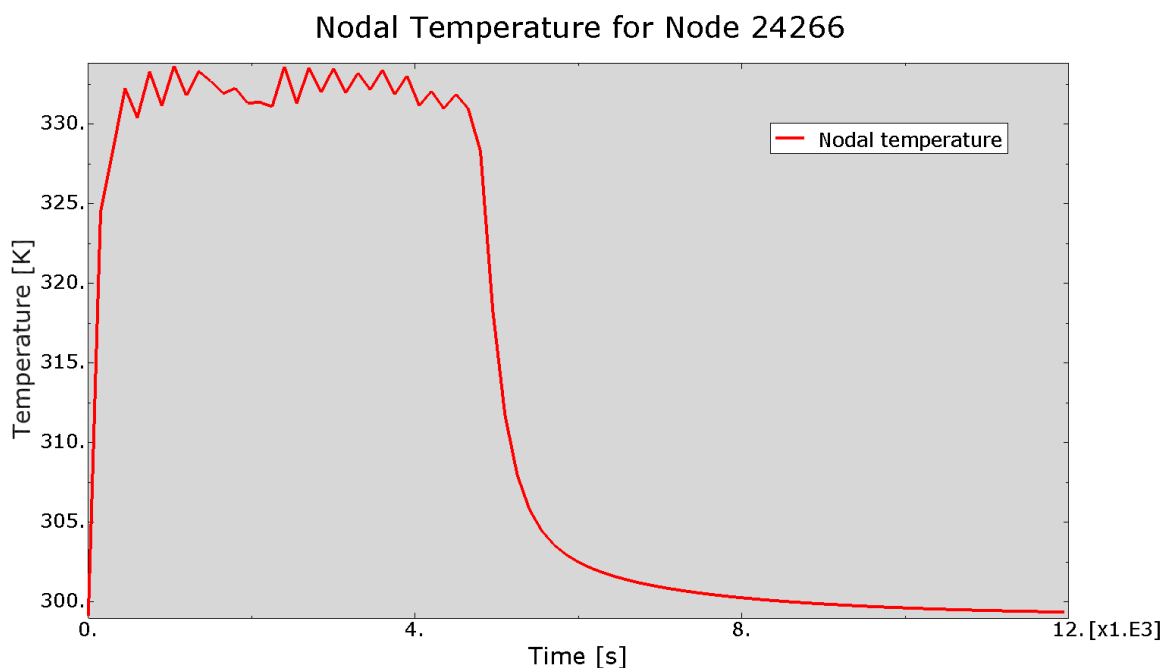


Figure 4.11: The nodal temperature of node 24266 during a printing process with a cooling time of 120 minutes.

The nodal temperature can be seen in Figure 4.11. At about 8000 s the temperature has dropped down to about 300 K and decreases slowly in the remaining time. The 8000 s

account for a cooling time of approximately 55 minutes. The difference if considering 40-minute cooling (around 7100 s) as was done for the increment sensitivity analysis is still quite small and does not affect the final results by more than approximately ± 10 MPa as visible if the results reported above are compared. A shorter cooling time can therefore easily be considered without affecting the final results much but improving the computational time.

4.2 Single track

4.2.1 Reference results

The results of the reference configuration for the single-track simulation can be seen in Figure 4.12.

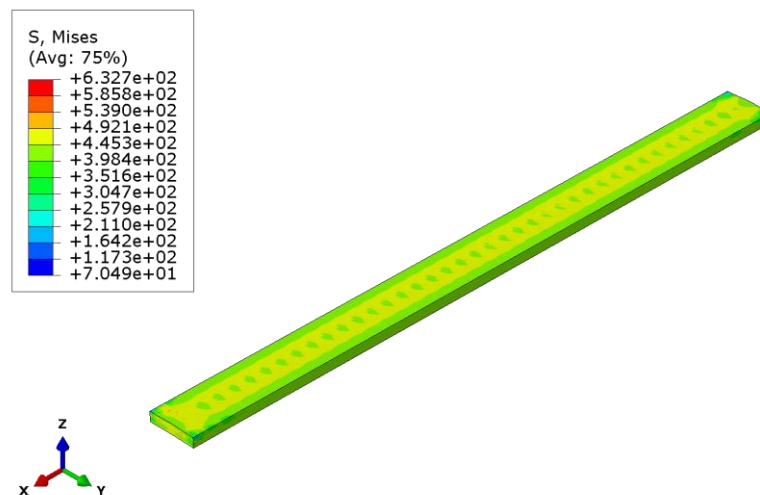


Figure 4.12: Predicted Mises stress of the single track for the reference configuration for averaged values. The effects of the increment size are visible in the centre of the track.

The maximum stress reported is about 632.7 MPa with interpolated values. The element-based quilt representation shows lower values down to 506.3 MPa as visible in the following sections. The effects of the increment sizes are clearly visible in the centre of the track indicating that smaller increments should be used to get more accurate results.

The lower stress at the edge of the track can partially be explained by the melt pool size. The melt pool size changes with the changing parameters but to keep the model simple the width of the track was kept the same for all runs. The melting range of the material is between 1260-1355 °C [15] so by taking the approximate average of 1300 °C and highlighting regions with higher temperature the expected melt pool can be visualized. In Figure 4.13 the approximate melt pool size for the reference configuration is shown and as visible the width of the melt pool does not equal the width of the track so the stresses caused by the laser

heating would be lower in that area since it does not experience as high temperature gradients as the rest of the track.

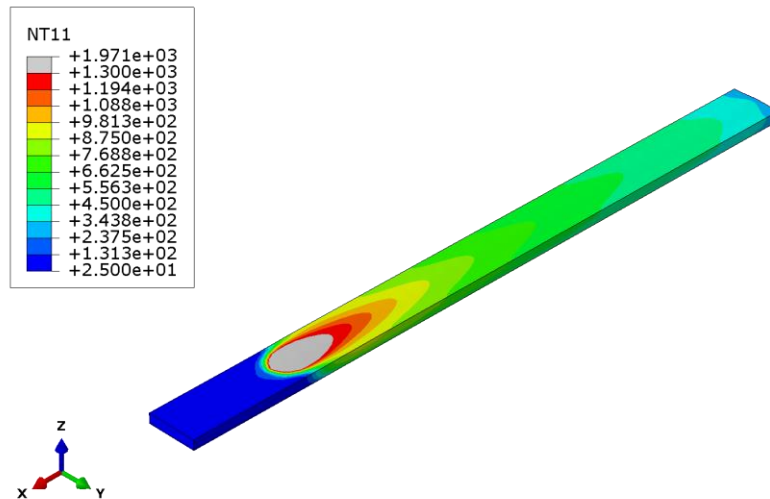


Figure 4.13: Approximate melt pool size for the reference configuration of the single-track simulation.

The expected effects on the melt pool size due to change in the process parameters is demonstrated in Figure 4.14 where the melt pool size is shown for three different laser power. For the highest laser power, the melt pool reaches the edges of the track but that is not the case for the other two power settings. With the lowest laser power sufficient melt pool depth to fuse to the substrate also becomes a question. The change in the melt pool size is most prominent for different power settings but different size is observed for all parameters varied in the sensitivity analysis that follows.

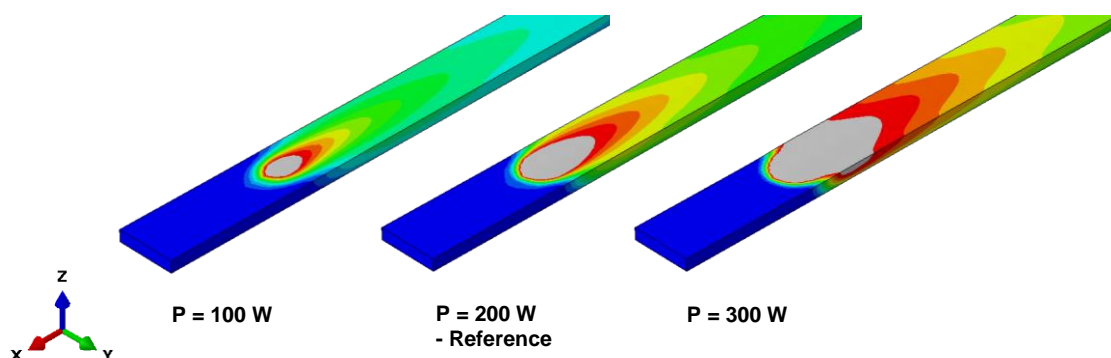


Figure 4.14: An example of how the melt pool size changes with varying properties. On the left the approximate melt pool size for $P = 100$ W, in the centre for $P = 200$ W and on the right for $P = 300$ W. The change observed in the melt pool size was most prominent for the change in power.

To investigate the stresses that form in the track further the nodal temperature, Mises stress and pressure of a node at the centre of the track are plotted over a part of the process time. The node is number 6792 and shown in Figure 4.15.

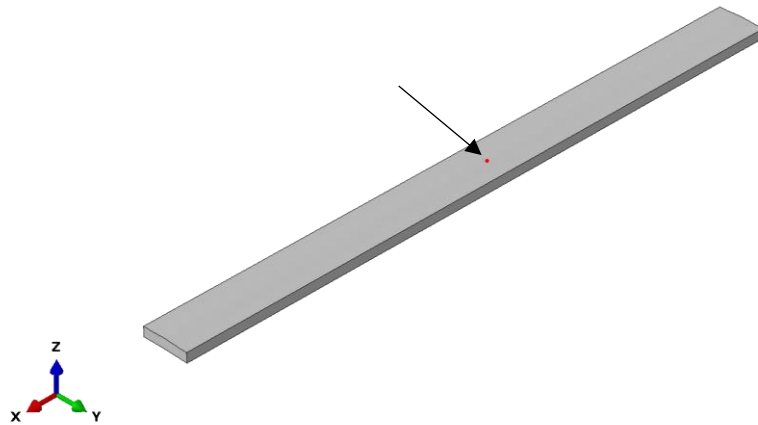


Figure 4.15: The location of node 6792 on the single track marked with a small red dot, pointed out by the arrow.

The resulting plot is shown in Figure 4.16. As the nodal temperature increases the stress is formed in the part. At first, during the heating up of the material when it is expanding the stress is compressive as can be seen by the positive pressure presented in the graph. As the temperature starts decreasing however, the stress decreases again as the pressure goes down to zero and as the material contracts the pressure becomes negative which indicates the change to tensile stress formation.

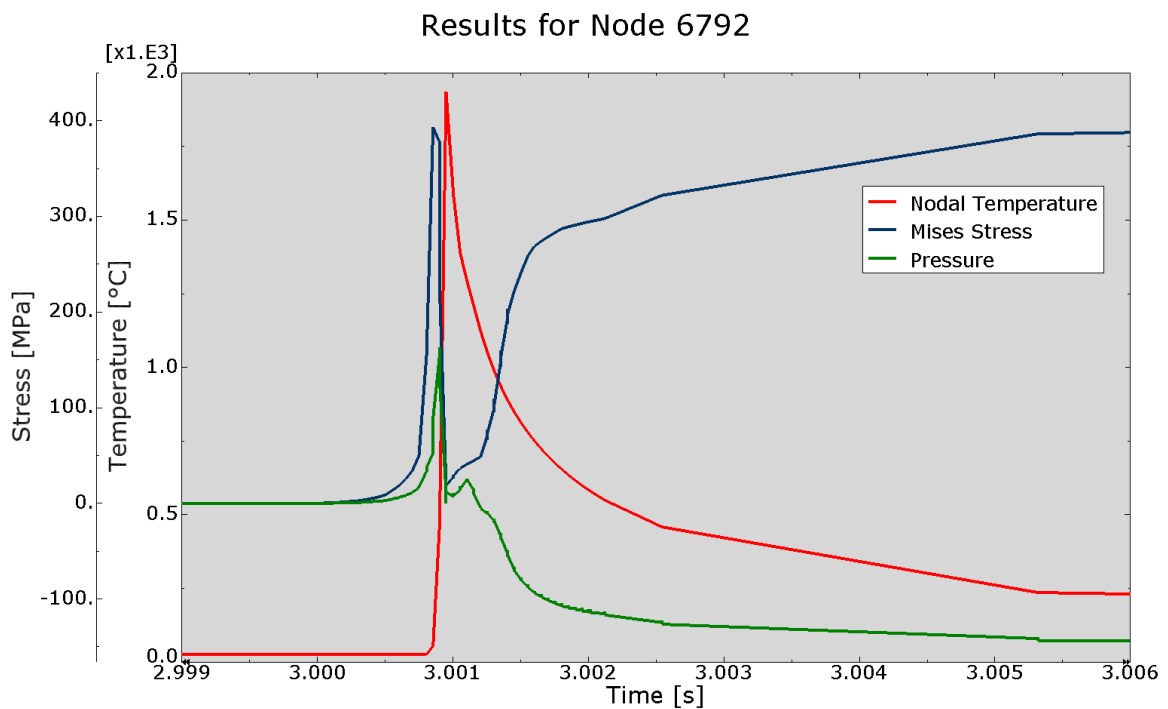


Figure 4.16: Nodal temperature, Mises stress and pressure for node 6792 during part of the printing process.

4.2.2 Sensitivity analysis

It should be noted that the stress analysis for some of the runs did not finish due to unknown reasons but they all stopped after the system was very close to equilibrium so it should not affect the comparability of the results.

Power

When the laser power is varied in the single-track simulation the predicted residual stresses increase with an increase in laser power, counter to what was reported for the increased power in the bridge simulation. The resulting stress profiles and maximum stresses reported can be viewed in Figure 4.17.

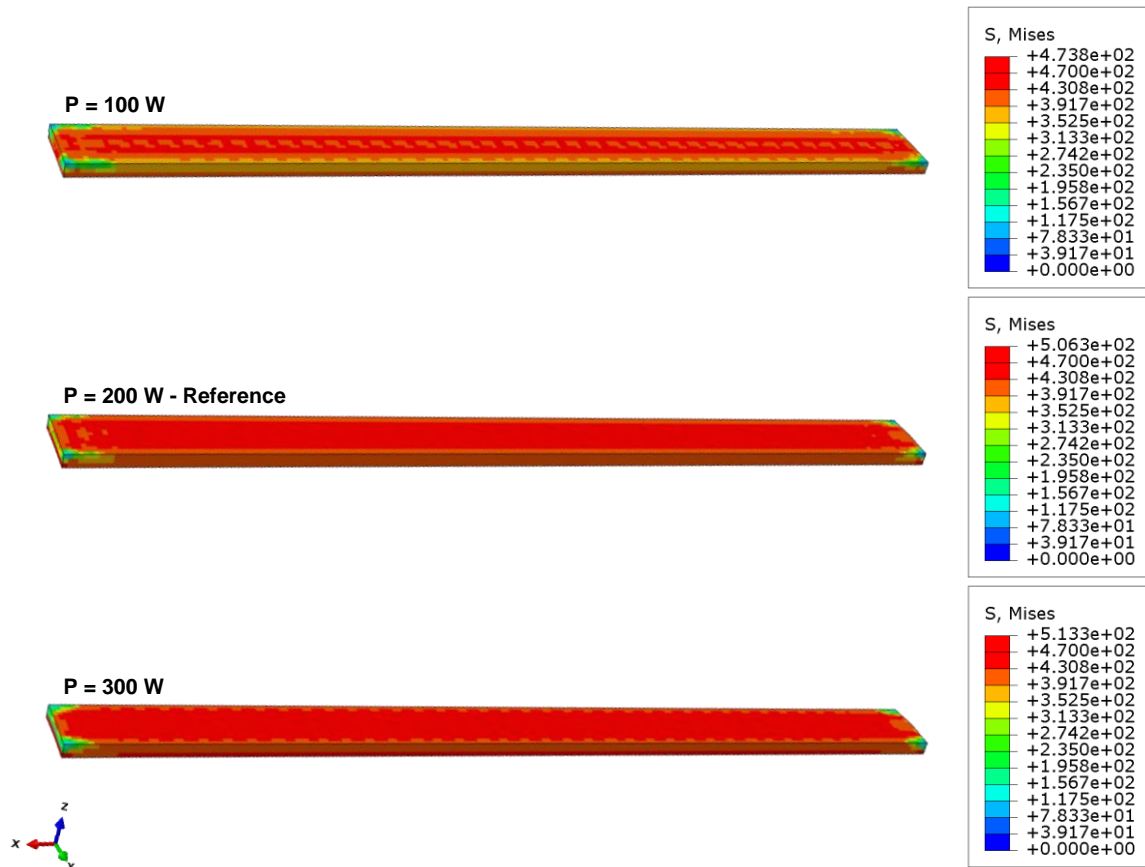


Figure 4.17: The predicted Mises stress profiles of the single track for three different laser power. A laser power of 100 W is shown at the top, 200 W in the centre and 300 W at the bottom. The stress increases with increasing laser power, in contrast to what is reported for the bridge simulation.

To explain these results, we investigate the temperature gradient along the track during an increment where the laser is close to the end of the track. The status of the print and the path along which the temperature gradient is investigated are shown in Figure 4.18. The temperature gradient is plotted as a function of distance along the track, starting close to the centre of the melt-pool in the saddle point where the temperature gradient changes direction,

and along the majority of the track to the end where the laser started. The graph showing the temperature gradient for the three different laser power can be viewed in Figure 4.19. The temperature gradient for the highest power of 300 W is highest for most of the track. A high temperature gradient results in higher residual stress formation due to the different cooling rates which can explain the trend observed in Figure 4.17.

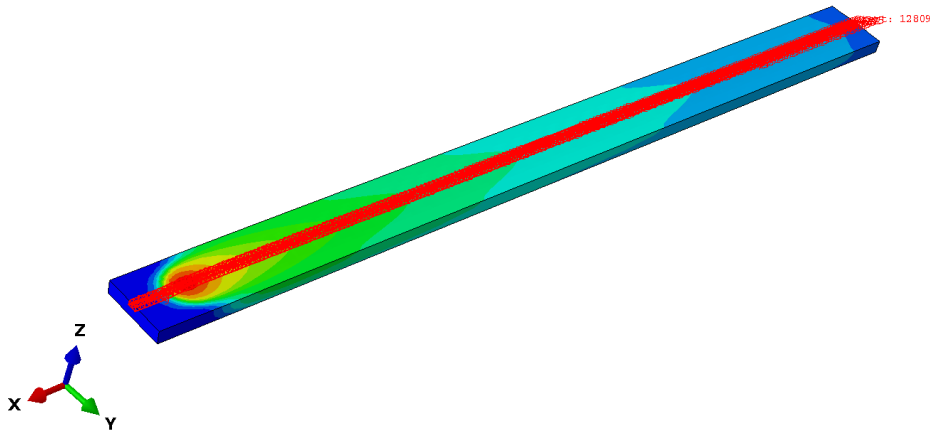


Figure 4.18: A path along the centre of printed track during at a point in time where the laser is close to the end of the track.

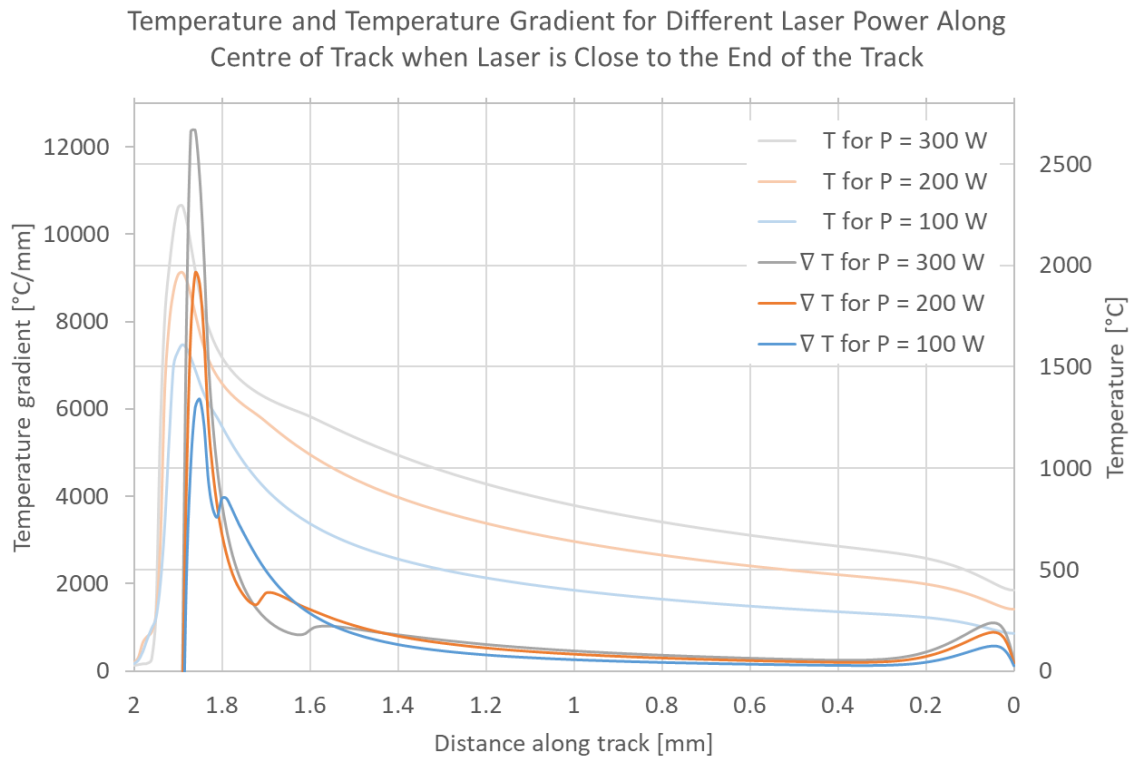


Figure 4.19: Graph showing the temperature gradient for three different laser power along the path shown in Figure 4.18. The temperature gradient is highest for the highest laser power along most of the track. The temperature for the different power is also shown.

Scan speed

The results for the predicted Mises stress for three different scan speeds can be viewed in Figure 4.20. The increase in scan speed leads to a decrease in the temperature gradient shown in Figure 4.21 for the same path as in the previous section which can be seen in Figure 4.18. This is again in contrast to what is reported for the bridge simulation.

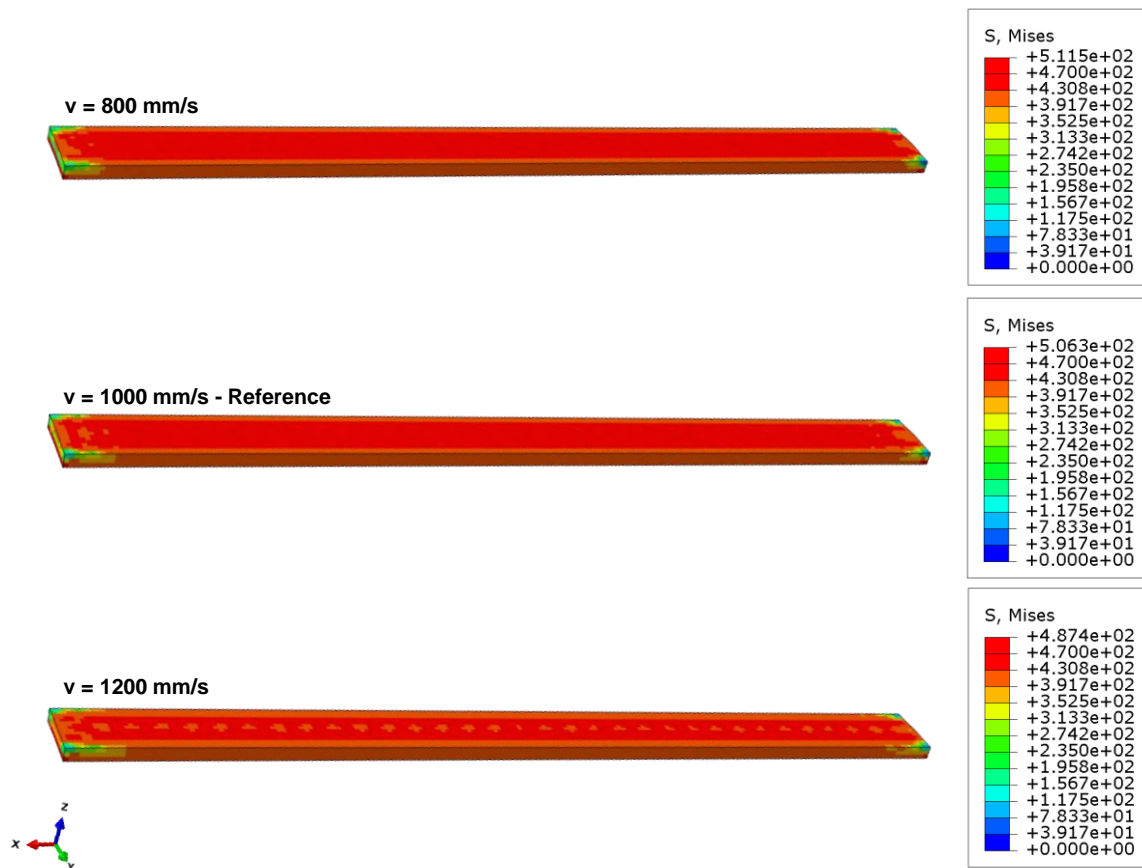


Figure 4.20: The predicted Mises stress profiles of the single track for three different scan speeds. A scan speed of 800 mm/s is shown at the top, the reference of 1000 mm/s in the centre and 1200 mm/s at the bottom. The stress decreases with increasing scan speed, in contrast to what is assumed for the bridge simulation.

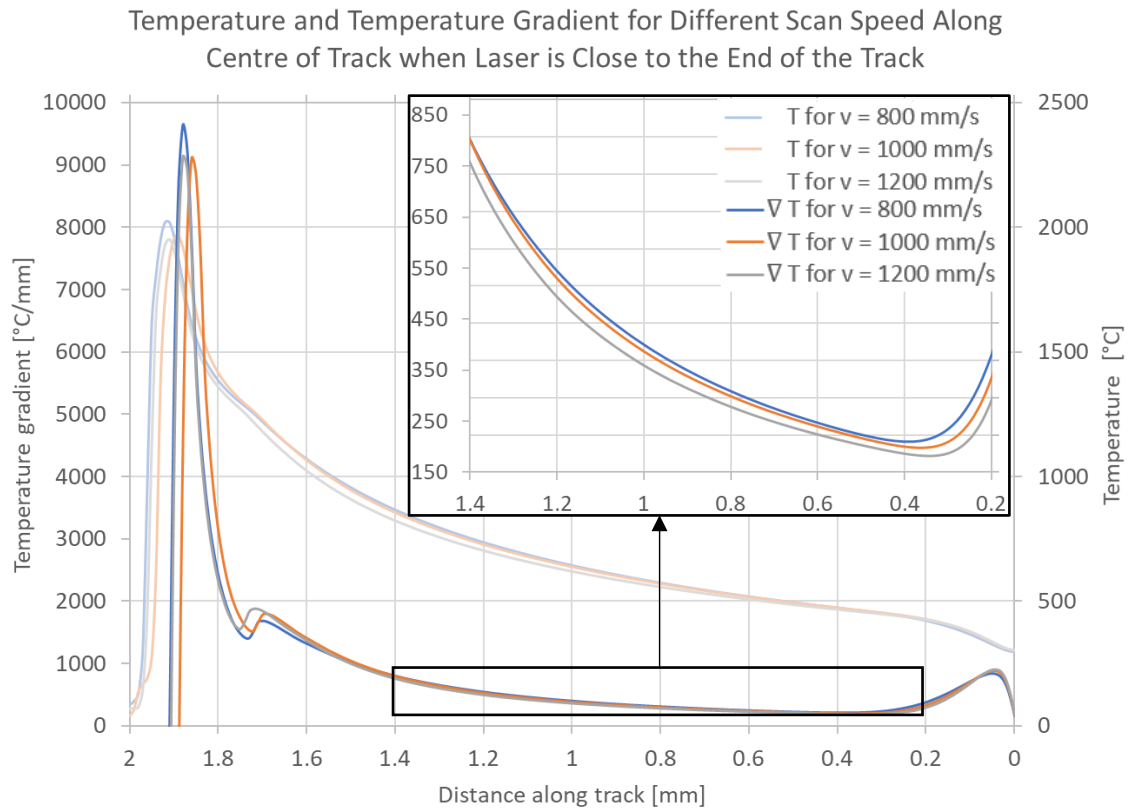


Figure 4.21: Graph showing the temperature gradient for three different scan speeds along the path shown in Figure 4.18. The temperature gradient is highest for the lowest scan speed along most of the track. The temperature for the different scan speeds is also shown.

Preheating temperature

For the preheating temperature the predicted Mises stress can be viewed in Figure 4.22. As the preheating temperature is increased, we observe a decrease in the maximum stress output similarly to what was reported for the bridge. The temperature gradient shown in Figure 4.23 confirms the observations by showing the temperature gradient for the reference case with no preheating having the highest values along the path.

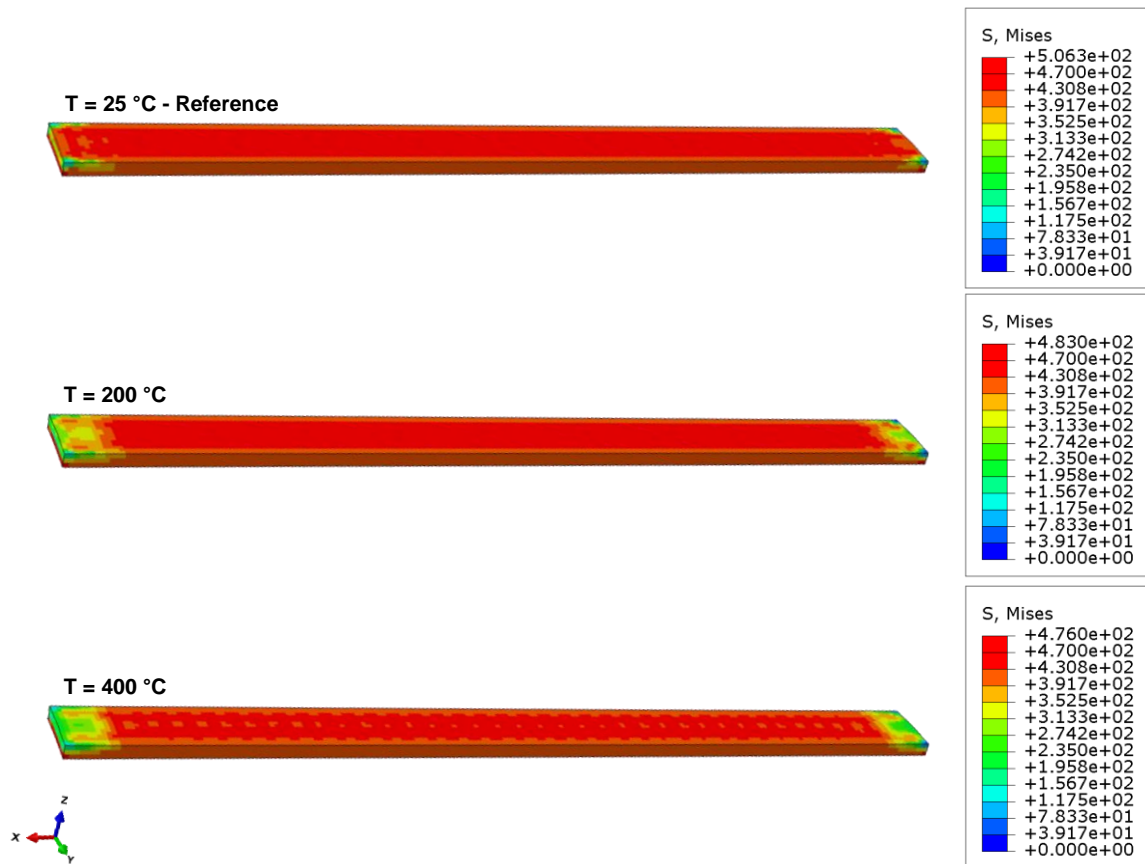


Figure 4.22: The predicted Mises stress profiles of the single track for three different initial temperatures. The reference of no preheating is shown at the top, an initial temperature of $T = 200$ °C in the centre and a preheating of $T = 400$ °C at the bottom. The stress decreases with increasing scan speed in accordance with what is predicted for the bridge simulation.

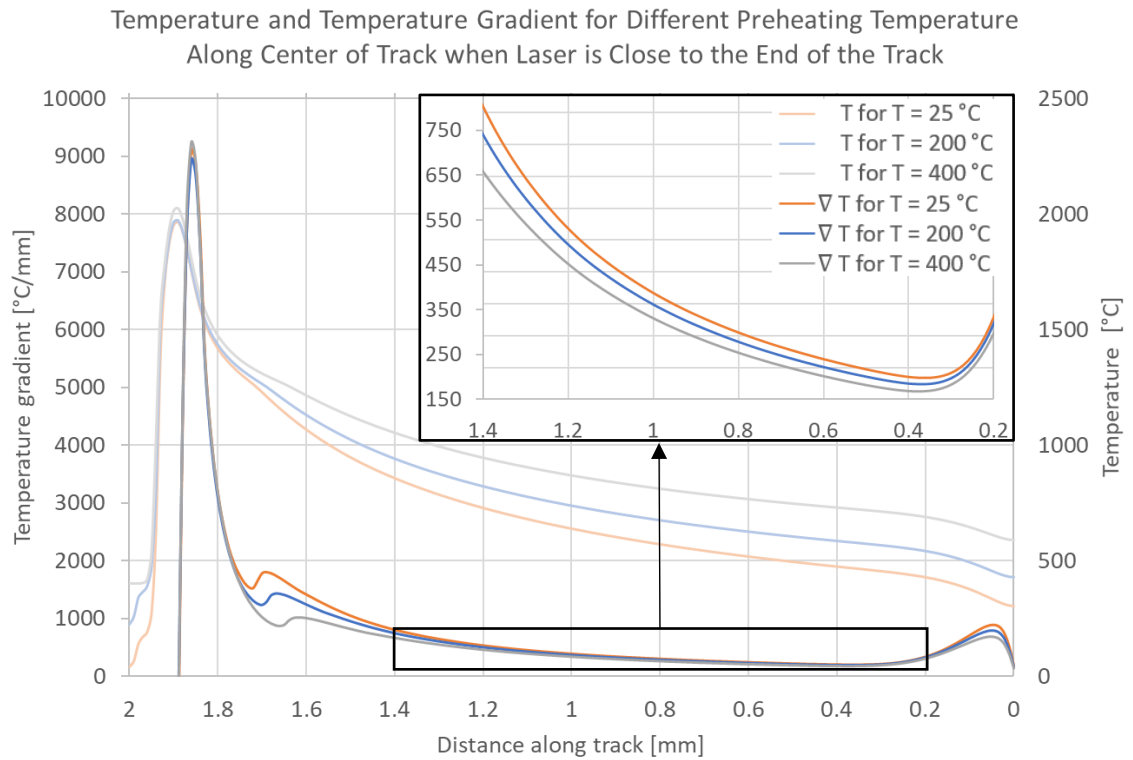


Figure 4.23: Graph showing the temperature gradient for three different initial temperatures along the path shown in Figure 4.18. The temperature gradient is highest for the lowest initial temperature along most of the track. The temperature for the different preheating temperatures is also shown.

5 Conclusions

When the results for the two different simulation scales are compared, we see that the results are not in agreement with each other. In Table 5.1 the effects of increasing the value of the various parameters are taken together for both simulations. As indicated there the results of the bridge and single-track simulation disagree on the effects of power and scan speed but agree on the effects of preheating. The single-track results of increasing residual stresses with increasing laser power are in accordance with the results reported by Waqar et al. [6] and Mugwagwa et al. [14] but according to them an increase in scan speed should also lead to increasing residual stresses which is not the case for the single track. The opposite goes for the bridge simulation where an increase in scan speed is assumed to lead to an increase in residual stress formation but then an increase in power leads to a decrease in the residual stresses.

Table 5.1: The effects of increasing the value of different process parameters such as laser power, scan speed, preheating temperature and relaxation temperature for both simulation models.

Parameter	RS Bridge	RS Single Track
↑ Power	↓	↑
↑ Scan speed	(↑)	↓
↑ Preheating T	↓	↓
↑ Relaxation T	↑	-

The results for decreasing residual stresses with increasing preheating temperature are in agreement for both sensitivity analyses and in accordance with the trends observed in the literature [1]. An increase in residual stress formation with an increase in relaxation temperature as observed in the bridge simulation is also in accordance with the literature [2].

A part of the results therefore seems to give us a clue about the effects the parameters have on the formation of residual stresses while the other parts demonstrate the complexity of the process and emphasizes the need for further research and experimental validation.

The AM Modeler – Plug-in uses thermal contractions to calculate the residual stresses in the parts and does not rely on plastic deformations since residual stresses can form in parts without plasticity modelled. The values for the residual stresses predicted by the plug-in vary somewhat by the input parameters. They should therefore be taken with care, but the overall stress distribution and stress peaks seem like a more useful output of the tool at this moment.

It should be noted that for the single-track simulation all temperatures were input in °C. This is not accurate since a radiation effect is used in the calculations and the temperatures should therefore have been input in Kelvins.

Outlook

These results show that even though there is an indication that some parameters affect the printing process in a certain way more research is needed to determine the true relationship between the many variables of the AM printing processes.

For continued research in relation to the models presented here many things could be considered, including the following.

- Comparing sensitivities for different parameters to identify the most sensitive parameters.
- Further study on effects of plasticity on the models.
- Further research and interpretation of the effects of the increment size on predicted results.
- Experimental comparison and calibration.

Further research with bigger changes in the model might include introducing more tracks or layers to the process level simulation to investigate the effects of the reheating of the deposited track as the adjacent tracks are printed as well as introducing new process parameters such as hatch spacing. In the simulations considered here the difference between the powder, liquid and solid state of the material is not specifically modelled with field variables which might also be an interesting thing to consider in future research.

References

- [1] P. Mercelis and J. P. Kruth, "Residual stresses in selective laser sintering and selective laser melting," *Rapid Prototyping Journal*, vol. 12, no. 5, pp. 254-265, 2006, doi: 10.1108/13552540610707013.
- [2] X. Song *et al.*, "Advances in additive manufacturing process simulation: Residual stresses and distortion predictions in complex metallic components," *Materials & Design*, vol. 193, p. 108779, 2020/08/01/ 2020, doi: <https://doi.org/10.1016/j.matdes.2020.108779>.
- [3] Fraunhofer Institute for Laser Technology ILT. "Process Development for Selective Laser Melting." <https://www.ilt.fraunhofer.de/en/media-center/brochures/b-process-development-for-slm.html> (accessed June 14, 2021).
- [4] H. Schleifenbaum, A. Diatlov, C. Hinke, J. Bültmann, and H. Voswinckel, "Direct photonic production: towards high speed additive manufacturing of individualized goods," *Production Engineering*, vol. 5, no. 4, pp. 359-371, 2011/08/01 2011, doi: 10.1007/s11740-011-0331-0.
- [5] S. Bremen, W. Meiners, and A. Diatlov, "Selective Laser Melting," *Laser Technik Journal*, vol. 9, no. 2, pp. 33-38, 2012, doi: <https://doi.org/10.1002/latj.201290018>.
- [6] S. Waqar, K. Guo, and J. Sun, "FEM analysis of thermal and residual stress profile in selective laser melting of 316L stainless steel," *Journal of Manufacturing Processes*, vol. 66, pp. 81-100, 2021/06/01/ 2021, doi: <https://doi.org/10.1016/j.jmapro.2021.03.040>.
- [7] Dassault Systemes. "Abaqus Analysis Guide." https://help.3ds.com/2020/English/DSSIMULIA_Established/SIMACAEANLRefMap/simaanl-c-ov.htm?ContextScope=all&id=01da146e671b456f83df726b5d1e1e2b#Pg0 (accessed April 13, 2021).
- [8] Dassault Systemes. (2017). Lesson 2: New Data Structures [PowerPoint Slides].
- [9] N. An, G. Yang, K. Yang, J. Wang, M. Li, and J. Zhou, "Implementation of Abaqus user subroutines and plugin for thermal analysis of powder-bed electron-beam-melting additive manufacturing process," *Materials Today Communications*, vol. 27, p. 102307, 2021/06/01/ 2021, doi: <https://doi.org/10.1016/j.mtcomm.2021.102307>.
- [10] R. Mertens, S. Dadbakhsh, J. V. Humbeeck, and J. P. Kruth, "Application of base plate preheating during selective laser melting," *Procedia CIRP*, vol. 74, pp. 5-11, 2018/01/01/ 2018, doi: <https://doi.org/10.1016/j.procir.2018.08.002>.
- [11] Q. Liu, Y. Danlos, B. Song, B. Zhang, S. Yin, and H. Liao, "Effect of high-temperature preheating on the selective laser melting of yttria-stabilized zirconia ceramic," *Journal of Materials Processing Technology*, vol. 222, pp. 61-74, 2015/08/01/ 2015, doi: <https://doi.org/10.1016/j.jmatprotec.2015.02.036>.
- [12] P. Promopattum and S.-C. Yao, "Influence of scanning length and energy input on residual stress reduction in metal additive manufacturing: Numerical and experimental studies," *Journal of Manufacturing Processes*, vol. 49, pp. 247-259, 2020/01/01/ 2020, doi: <https://doi.org/10.1016/j.jmapro.2019.11.020>.
- [13] Z. Xiao *et al.*, "Study of residual stress in selective laser melting of Ti6Al4V," *Materials & Design*, vol. 193, p. 108846, 2020/08/01/ 2020, doi: <https://doi.org/10.1016/j.matdes.2020.108846>.
- [14] L. Mugwagwa, I. Yadroitsev, and S. Matope, "Effect of Process Parameters on Residual Stresses, Distortions, and Porosity in Selective Laser Melting of Maraging Steel 300," *Metals*, vol. 9, no. 10, p. 1042, 2019. [Online]. Available: <https://www.mdpi.com/2075-4701/9/10/1042>.
- [15] I. Haynes International, "Hastelloy® X Alloy", U.S.A, Brochure 1997.
- [16] J. J. Valencia and P. N. Quested, "Thermophysical Properties," vol. 15, *ASM Handbook Volume 15: Casting*, 2008, pp. 468-481. [Online]. Available: <http://hdl.handle.net/11115/166>
- [17] Z. Luo and Y. Zhao, "Efficient thermal finite element modeling of selective laser melting of Inconel 718," *Computational Mechanics*, vol. 65, no. 3, pp. 763-787, 2020/03/01 2020, doi: 10.1007/s00466-019-01794-0.
- [18] M. Shunmugavel, A. Polishetty, and G. Littlefair, "Microstructure and Mechanical Properties of Wrought and Additive Manufactured Ti-6Al-4V Cylindrical Bars," *Procedia Technology*, vol. 20, pp. 231-236, 2015/01/01/ 2015, doi: <https://doi.org/10.1016/j.protcy.2015.07.037>.



Declaration of originality

The signed declaration of originality is a component of every semester paper, Bachelor's thesis, Master's thesis and any other degree paper undertaken during the course of studies, including the respective electronic versions.

Lecturers may also require a declaration of originality for other written papers compiled for their courses.

I hereby confirm that I am the sole author of the written work here enclosed and that I have compiled it in my own words. Parts excepted are corrections of form and content by the supervisor.

Title of work (in block letters):

RESIDUAL STRESS PREDICTION IN SLM PARTS: A SENSITIVITY ANALYSIS

Authored by (in block letters):

For papers written by groups the names of all authors are required.

Name(s):

TRYGGVADOTTIR

First name(s):

THORDIS

With my signature I confirm that

- I have committed none of the forms of plagiarism described in the 'Citation etiquette' information sheet.
- I have documented all methods, data and processes truthfully.
- I have not manipulated any data.
- I have mentioned all persons who were significant facilitators of the work.

I am aware that the work may be screened electronically for plagiarism.

Place, date

Zürich, 21.06.21.

Signature(s)

Pórdís Tryggvadóttir

For papers written by groups the names of all authors are required. Their signatures collectively guarantee the entire content of the written paper.